HHS Public Access

Author manuscript

J Comp Neurol. Author manuscript; available in PMC 2021 November 01.

Published in final edited form as:

J Comp Neurol. 2020 November 01; 528(16): 2748–2766. doi:10.1002/cne.24929.

Expression profiling of precuneus layer III cathepsin D-immunopositive pyramidal neurons in mild cognitive impairment and Alzheimer's disease: Evidence for neuronal signaling vulnerability

Bin He[1], **Sylvia E. Perez**[1], **Sang Han Lee**[2,3], **Stephen D. Ginsberg**[4,5,6,7], **Michael Malek-Ahmadi**[8], **Elliott J. Mufson**[1]

[1]Department of Neurobiology and Neurology, Barrow Neurological Institute, Phoenix, Arizona

[2]Center for Biomedical Imaging and Neuromodulation, Nathan Kline Institute, Orangeburg, New York

[3]Child and Adolescent Psychiatry, New York University School of Medicine, New York, New York

[4]Center for Dementia Research, Nathan Kline Institute, Orangeburg, New York

[5]Department of Psychiatry, New York University School of Medicine, New York, New York

[6]Neuroscience & Physiology, New York University School of Medicine, New York, New York

[7]NYU Neuroscience Institute, New York University School of Medicine, New York, New York

[8]Banner Alzheimer's Institute, Phoenix, Arizona

Abstract

The precuneus (PreC; Brodmann area 7), a key hub within the default mode network (DMN) displays amyloid and tau-containing neurofibrillary tangle (NFT) pathology during the onset of Alzheimer's disease (AD). PreC layer III projection neurons contain lysosomal hydrolase cathepsin D (CatD), 14)a marker of neurons vulnerable to NFT pathology. Here we applied single population laser capture microdissection coupled with custom-designed microarray profiling to determine the genetic signature of PreC CatD-positive-layer III neurons accrued from postmortem tissue obtained from the Rush Religious Orders Study (RROS) cases with a premortem clinical diagnosis of no cognitive impairment (NCI), mild cognitive impairment (MCI) and AD. Expression profiling revealed significant differential expression of key transcripts in MCI and AD compared to NCI that underlie signaling defects, including dysregulation of genes within the endosomal-lysosomal and autophagy pathways, cytoskeletal elements, AD-related genes, ionotropic and metabotropic glutamate receptors, cholinergic enzyme and receptors, markers of monoamine neurotransmission as well as steroid-related transcripts. Pervasive defects in both MCI

Address correspondence to: Elliott J. Mufson, PhD, Alzheimer's and Brain Trauma Research Laboratory, Institutional Professor, Greening Chair in Neuroscience, Barrow Neurological Institute, 350 W. Thomas Rd, Phoenix, AZ 85013, elliott.mufson@dignityhealth.org phone: 602-406-8525, Fax: 602-406-8520.

Conflict of Interest: Authors have no conflict of interest to declare.

Data Sharing and Data Accessibility: The data that support the findings of this study are available on request from the corresponding author. These data are not publicly available due to privacy or ethical restrictions.

and AD were found in select transcripts within these key gene ontology categories, underscoring the vulnerability of these corticocortical neurons during the onset and progression of dementia. Select PreC dysregulated genes detected via custom-designed microarray analysis were validated using qPCR. In summary, expression profiling of CatD positive PreC layer III neurons revealed significant dysregulation of a mosaic of genes in MCI and AD that were not previously appreciated in terms of their indication of systems-wide signaling defects in a key hub of the DMN.

Keywords

Alzheimer's disease; expression profiling; laser capture microdissection; mild cognitive impairment; microarray; neurons; precuneus; RRID

Introduction

The precuneus [PreC; Brodmann area 7 (BA7)], a key component of the default mode network (DMN), which plays a role in episodic memory retrieval (Wagner et al., 2005), displays high metabolic activity during conscious rest and selectively deactivates during non-self-directed cognitive tasks in the healthy human brain (Buckner et al., 2008; Raichle et al., 2001; Sperling et al., 2010). By contrast, the PreC is dysregulated in aging (Andrews-Hanna et al., 2007), inactivates during cognitive tasks and is compromised during the early stages of Alzheimer's disease (AD) (Herholz et al,. 2002; Matsuda., 2007; Rombouts et al., 2005). Pittsburgh Compound B ([^{3}H]PiB) amyloid imaging demonstrates the DMN is prone to amyloid-beta peptide (Aβ) deposition in the earliest preclinical stages of AD (Mintun et al., 2006; Sheline et al., 2010; Sperling et al., 2009). The PreC also displays a greater degree of atrophy in early compared to late-onset AD (Frisoni et al., 2005; Ishii et al., 2005; Karas et al., 2007), a reduction in synapse number in AD but not in mild cognitive impairment (MCI) (Scheff et al., 2013) and a relationship between synaptic failure, functional and structural disconnection, and amyloid deposition prior to the onset of dementia (Drzezga et al., 2011; Yan et al., 2013). Despite extensive amyloid PiB binding, neurofibrillary tangle (NFT) bearing neurons are relatively sparse in the PreC compared to other vulnerable hubs of the DMN (Nelson et al., 2009; Perez et al., 2015). Currently, molecular factors associated with PreC neuron dysfunction during the onset of AD remain under investigated.

Dysregulation of the endosomal-lysosomal (EL) system is an early event in the pathogenesis of neocortical (Cataldo et al., 1995), hippocampal, and cholinergic basal forebrain neurons in prodromal AD (Ginsberg et al., 2000, 2010, 2011), which precedes amyloid and tau pathology (Cataldo et al., 1997). Numerous studies indicate the EL system plays a key role in amyloid-β precursor protein (APP) processing and Aβ generation in AD (Pasternak et al., 2004; Nixon, 2007, 2017). Vulnerable neurons display an increase in the size and number of lysosomes containing cathepsin D (CatD) (Cataldo et al., 1997), a ubiquitous and abundant lysosomal hydrolase. Transcriptomic and protein based assays demonstrate upregulation of *CatD* mRNA and protein levels in hippocampal and neocortical layer III and V pyramidal neurons in AD, including NFT-pyramidal neurons (Ginsberg et al., 2000; Cataldo et al., 1996), indicating an increase in the activation of the EL system in neurons prone to tau

pathology (Ginsberg et al., 2010; Cataldo et al., 1995). CatD mediates programed cell death (Deiss et al., 1996) and carriers of the T-allele of rs17571 located on the *CatD* gene show an increased risk for AD (Riemenschneider et al., 2006). Genetic ablation of *CatD* markedly potentiates tau-induced neurotoxicity, indicating a role for this encoded protein in neuroprotection (Khurana et al., 2010). In the present study, we investigated the genetic signature of PreC CatD-positive layer III neurons in tissue obtained from participants in the Rush Religious Orders Study (RROS) that died with a premortem clinical diagnosis of no cognitive impairment (NCI), MCI, or AD. These findings will aid in understanding the mechanisms underlying cortical cellular neurodegeneration and potential resilience to disease within the DMN memory and executive function circuit.

Materials and Methods

Subjects

A total of 31 cases with an antemortem clinical diagnosis of NCI (n=11, 8F/3M, 86.17 ± 4.95 years), MCI (n=11, 9F/2M, 87.36 ± 4.58 years), and AD (n=9, 6F/3M, 88.48± 5.36 years) from the RROS (Mufson et al., 1999; Bennett et al., 2005, 2006) were examined (Table 1). Each participant agreed to an annual detailed premortem clinical evaluation, brain donation at the time of death and a postmortem neuropathological evaluation. Written informed consent for research and autopsy was obtained from family or guardians of each subject participating in the study. The Human Investigations Committee of Rush University Medical Center approved the study.

Clinical and Neuropathological Evaluation

Clinical, demographic and neuropathological case details are reported in Table 1. Clinical evaluation and criteria for diagnosis of AD and MCI have been published previously (Mufson et al., 1999; Bennett et al., 2005; Davis et al., 1999; Perez et al., 2012; Schmitt et al., 2012). Briefly, following review of clinical data and participant examination, clinical diagnoses were made by a board-certified neurologist with expertise in gerontology. A neurologist reviewed medical history, medications, findings from neurologic examinations, cognitive performance scores and the neuropsychologist's opinion of cognitive impairment and the presence of dementia. Each subject was evaluated in their home, emphasizing clinically relevant findings. AD diagnosis of dementia followed the recommendations of the joint working group of the National Institute of Neurological and Communicative Disorders and the Stroke and the Alzheimer's Disease and Related Disorders Association (NINCDS/ADRDA) (McKhann et al., 1984). Clinical classification of MCI are compatible with those used by others in the field to describe persons who are not cognitively normal, but do not meet accepted criteria for dementia (Rubin et al., 1989; Petersen et al., 1995; Ebly et al., 1995; Devanand et al., 1997; Albert et al., 1991; Flicker et al., 1991). MCI was defined as persons rated as impaired on neuropsychological testing by a neuropsychologist but not found to have dementia by the examining neurologist. Average time from the last clinical evaluation to death was ~8 months.

Among the MCI cases, five are amnestic (45.5%) and six are non-amnestic (54.5%) (Schmitt et al., 2000). The Mini-mental status exam (MMSE) and a neuropsychological battery was

also available within two years prior to death, from which a global cognitive *z*-score (GCS) comprised of 19 individual tests was computed, as was an episodic memory *z*-score (Albert et al., 1991) based on seven tests (East Boston Memory immediate and delayed recall, Logical Memory immediate and delayed story recall, CERAD Word List Memory immediate and delayed recall, and CERAD Word List Recognition). At a consensus conference a neurologist and neuropsychologist reviewed all clinical data, medical records, interviews with family members and assigned a final clinical diagnosis for each subject. Postmortem neuropathological diagnosis was performed as reported previously (Mufson et al., 1999; Bennett et al., 2005; Perez et al., 2012; Schmitt et al., 2012), which included NIA-Reagan criteria (Newell et al., 1999), recommendations of the CERAD (Mirra, 1997), Braak staging of NFTs, amyloid deposition scores (Braak & Braak, 1991) and TDP-43 reactivity (Josephs et al., 2016). Cases with other pathologies (e.g., cerebral amyloid angiopathy, dementia with Lewy bodies, hippocampal sclerosis, Parkinson's disease, and large strokes) were excluded from the study. None of the subjects examined were treated with anticholinesterase inhibitors.

Brain samples

PreC tissue was dissected using fiduciary landmarks and fixed at autopsy in 4% paraformaldehyde (pH 7.4) for at least 5 days, cryoprotected in a solution containing 30% glycerol, 30% ethylene glycol, in 0.1 M phosphate buffer, cut in parallel series at 40 μm on a freezing sliding microtome and stored in the same cryoprotectant at −20 °C until processing (Perez et al., 2012; Mufson et al., 1997). Cortical slabs from the opposite hemisphere containing the PreC were snap frozen and kept at −80 ° C.

Immunohistochemistry

Floating PreC sections were washed in phosphate buffer and Tris-buffered saline (TBS) before a 20 min incubation in 0.1 M sodium metaperiodate (Sigma-Aldrich, St. Louis, MO) in TBS to inactivate endogenous peroxidase activity. Tissue sections were blocked in TBS containing 0.25% Triton-X 100 and 3% goat serum for 1 h. Sections were incubated with a mouse monoclonal to human CatD primary antibody generated from recombinant human Cathepsin D (21-412 aa) and purified using protein G (Lifespan Biosciences, Seattle, WA, Cat# LS-B2931 RRID:AB_1931140; 1:200 dilution). Western blotting detected a single band for CatD and did not cross react with other protein targets (Lifespan Biosciences). Sections were incubated overnight at room temperature in 0.25% Triton X-100, 1% goat serum TBS solution in a humidified chamber. Sections were washed in TBS containing 1% goat serum prior to a 1 h incubation with the biotinylated goat anti-mouse secondary antibody (1:200 dilution; Vector Laboratories Cat# PK-7100, RRID:AB_2336827). Following TBS washes, sections were incubated using the Vectastain ABC kit (Vector Laboratories, Burlingame, CA) for 1 h, rinsed in 0.2 M sodium acetate, 1.0 M imidazole buffer (pH 7.4) and developed in acetate-imidazole buffer containing 0.05% 3,3′-diaminobenzidine tetrahydrochloride (DAB, Sigma-Aldrich) and 1 gram nickel ammonium sulfate. The reaction was terminated in acetate-imidazole buffer. Sections were mounted on glass slides, dried overnight and dehydrated in 100% ethanol. Immunohistochemical controls consisted of the elimination of the primary antibody resulting in a lack of immunoreactivity. To avoid differences in staining across cases, we immunostained and

developed all the cases at the same time, which controls for batch to batch differences in antibodies and reagents. CatD positive neurons appeared dark blue-black in all cases examined (Fig. 1a–c).

Laser capture microdissection and Terminal Continuation (TC) RNA amplification

The procedure for laser capture microdissection (LCM) and TC RNA amplification combined with custom-designed microarray technology has been described previously (Che & Ginsberg, 2004; Alldred et al., 2008, 2009; Ginsberg, 2008). Briefly individual PreC CatD-immunopositive layer III pyramidal neurons were microdissected (Fig. 1d–e) using a Zeiss PALM LCM III instrument (Zeiss, Oberkochen, Germany). Thirty PreC CatD-positive layer III neurons were captured per reaction for population cell analysis (Alldred et al., 2008; Ginsberg & Che, 2005). A total of two reactions were performed per human brain. TC RNA amplification protocol is available at http://cdr.rfmh.org/pages/ginsberglabpage.html. Total RNA from captured cells was extracted using Trizol reagent (ThermoFisher Scientific, Waltham, MA) according to manufacturer's instruction. RNAs were first reverse transcribed into cDNA. After RNase H digestion and re-annealing of T7-TC primer to generate cDNAs with double-stranded regions at the primer interfaces, single stranded cDNA was purified using Ambion Ultra 0.5 mL centrifugal filters (UFC 503024, EMD Millipore, Billerica, MA). Hybridization probes were synthesized by *in vitro* transcription using ^{33}P incorporation in 40 mM Tris (pH 7.5), 6 mM $MgCl_2$, 10 mM NaCl, 2 mM spermidine, 10 mM DTT, 125uM ATP, GTP and CTP, 2.5 μM of cold UTP, 20 U of RNase inhibitor, 2 KU of T7 RNA polymerase (TH950K, Lucigen, Sommerset, WI), and 60 μCi of ^{33}P -UTP (Perkin-Elmer, Boston, MA) (Alldred et al., 2008; Ginsberg, 2008). The reaction was performed at 37 °C for 4 h. Radiolabeled TC RNA probes were hybridized to custom-designed cDNA arrays without further purification.

Custom-designed cDNA array platforms and hybridization

Array platforms consisted of 1 μg of linearized cDNA purified from plasmid preparations adhered to high-density nitrocellulose membrane (Hybond XL, GE Healthcare, Piscataway, NJ). Each cDNA and/or expressed sequence-tagged (EST) cDNA was verified by sequence analysis and restriction digestion. Human and some mouse clones were employed on the custom-designed array. Approximately 576 cDNAs/ESTs were utilized on the current array platform. Although the majority of genes are represented by one transcript on the array platform, several genes have representation at 3' and 5' regions. Following overnight hybridization at 42 °C, arrays were washed sequentially in 2X SSC/0.1% SDS, 1X SSC/0.1% SDS and 0.5X SSC/0.1% SDS for 15 min each at 37 °C and exposed to a phosphor screen for 24 hours and developed using a phosphor imager (GE Healthcare, Chicago, IL). All array phosphor images were adjusted to the same brightness and contrast levels for data acquisition and analysis.

Quantitative polymerase chain reaction (qPCR)

RNA was extracted from 75 mg of frozen dissected PreC tissue from NCI (n=9), MCI (n=9) and AD (n=8) cases. Total RNA was purified on a column with DNase I treatment using a PureLink RNA Mini Kit (12183018A, ThermoFisher Scientific) according to manufacturer's instructions. Total RNA was quantitated using Infinite M200 PRO (Tecan, Männedorf,

Switzerland). qPCR was carried out in triplicate on a real-time qPCR cycler Applied Biosystem QuantStudio 6 Flex (ThermoFisher Scientific) in 96 well optical plates with coverfilm using TaqMan Universal Master Mix II with no UNG (ThermoFisher Scientific) and TaqMan gene expression assays. Genes analyzed via qPCR and the respective specific primers are as follows: galanin receptor 1 (*GALR1*; Hs00175668_m1), BRCA1 associated protein-1 (*BAP1*; Hs01109276_g1), RNA binding motif protein 3 (*RBM3*; Hs00943160_g1), *RAB11A* (Hs00366449_g1), glyceraldehyde-3-phosphate dehydrogenase (*GAPDH*; Hs02758991_g1), *HOMER1* (Hs01029333_m1), G-protein gamma 2 (*GNG2*; Hs00828232_m1), metabotropic glutamate receptor 1 (*GRM1*; Hs00168250_m1), glucose transporter 5 (*SLC2a5*; Hs01086390_m1), tissue inhibitor of metalloproteinase 1 (*TIMP1*; Hs01092512_g1), ribosomal protein S6 kinase, 70kDa, polypeptide 1 (*RPS6KB1*; Hs00356367_m1) and choline acetyltransferase (*CHAT*; Hs00758143_m1) (Table 2) (ThermoFisher Scientific). qPCR conditions were as follows: one cycle at 95° C for 10 min and 40 cycles of 95 °C for 15 sec and 60 °C for 1 min.

Statistical analysis

Clinical and demographic characteristics (e.g., age, educational level, GCS, MMSE, and PMI) were compared using a one-way analysis of variance (ANOVA) with Bonferroni-type correction for pairwise comparisons (Ginsberg et al., 2006a, 2006b; Counts et al., 2007). Gender and ApoE allele status were assessed across clinical conditions using a Fisher's exact test. Neuropathologic classifications (NIA-Reagan, CERAD, and Braak scoring) were compared among clinical diagnostic groups by the Kruskal-Wallis test (Ginsberg et al., 2006a, 2006b). Hybridization signal intensity was determined utilizing ImageQuant software (GE Healthcare, Chicago, IL). Statistical procedures for custom-designed microarray analysis have been described in detail (Ginsberg et al., 2006a; Ginsberg, 2008). Briefly, expression of TC amplified RNA bound to each linearized cDNA (approximately 576 cDNAs/ESTs on the array) minus background was expressed as a ratio of the total hybridization signal intensity of the array (a global normalization approach). Global normalization effectively minimizes variation due to differences in the specific activity of the synthesized probe and the absolute quantity of probe (Ginsberg, 2008; Eberwine & Crino, 2001). These data do not allow the absolute quantitation of mRNA levels. However, an expression profile of relative changes in mRNA levels was generated. Relative changes in total hybridization signal intensity and percentage of cDNA clones above negative control were analyzed as described previously (Ginsberg et al., 2006a; Counts et al., 2007; SAS Institute Inc, 2004). Since multiple cells were measured in each subject, between-subject versus within-subject (between-cell) variation in gene expression was analyzed by variance component analysis and intraclass correlation coefficients (Ginsberg et al., 2006b). False discovery rate (FDR) was used to correct for multiple comparisons among the correlations. The FDR was applied to each domain separately so that the significance level adjustment was based on 23 comparisons. Real time PCR used *GAPDH* as a reference gene. Relative mRNA expression levels of target genes were calculated via $2^{-\Delta\Delta CT}$ method (Schmittgen & Livak, 2008). ANOVA on Ranks was used to analyze the significant difference of gene expression of qPCR. For microarray analysis, level of statistical significance was set at $p \leq 0.01$, p values between 0.01 and 0.05 were considered as a trend level (^{t}) (Ginsberg et al.,

2010, 2019; Alldred et al., 2018). For other analyses, the level of statistical significance was set at $p < 0.05$.

Results

Case demographics

Clinical groups did not differ by age (p=0.59), sex (p=0.74), education level (p=0.57), postmortem interval (PMI, p=0.27), or brain weight (p=0.83) (Table 1). There were significantly more cases with an ApoE ε4 genotype in MCI (45 %) and AD (28.6%) (p=0.04) compared to NCI (0%). MMSE (p<0.001), GCS (p<0.001), and episodic memory *z*-score (p<0.001) were significantly lower in AD compared to MCI and NCI. No significant differences were found for the Semantic Memory *z*-score (p=0.46), Working Memory *z*-score (p=0.25), and Visuospatial *z*-score (p=0.08) in AD compared to MCI and NCI. Significant differences for these cognitive variables were not found between NCI and MCI (Table 1). Neuropathological examination revealed that 89% of AD, 82% of MCI and 82% of NCI cases were Braak stage III-V. NIA-Reagan criteria revealed that 45% of NCI, 73% of MCI, and 89% of AD cases were classified as intermediate to high likelihood of AD. CERAD diagnosis revealed that 27% of NCI, 27% of MCI, and 33% of AD cases received a diagnosis of probable or definite AD. Among the three clinical diagnostic groups no differences were found in Braak scores (p=0.76), NIA-Reagan (p=0.17) or CERAD diagnosis (p=0.1) (Table 1). We divided the 11 NCI cases into those with low Braak scores (I-III; n=5) and high Braak score (IV-V; n=6) and found that only 3 genes (0.52%) {*USP8* (p=0.01), *AGER* (p=0.02[t]) and *PPP2CA* (p=0.04[t])} were significantly different (n=1) or trend-level different (n=2) between these NCI cases, suggesting that Braak score did not influence results in the NCI group. Interestingly, only 10 of 576 genes (1.73%) {*EIF2AK2* (p=0.001), *GNG2* (p=0.004), *ATG4D* (p=0.006), *RPS6KB1* (p=0.01), *MSR1* (p=0.02[t]), *GABRA6* (p=0.03[t]), *RAP1B* (p=0.03[t]), *MAPT2N6D* (p=0.05[t]), *TUBB2C* (p=0.05[t]), and *MAPT1N6P* (p=0.05[t])} were significant (n=4) or trend-level different (n=6) between non-amnestic and amnestic MCI subjects. Data for TDP 43 was available for a subset of the cases (n=23) examined. Of these cases TDP-43 accumulation was found in 4 NCI (stage 1, amygdala), 2 MCI (stage 1, amygdala) and 4 AD (stage 2-3, amygdala, entorhinal cortex, and subiculum) cases according to the recent schema for TDP 43 pathology (Josephs et al., 2016). Quantitative analysis did not reveal differences in average intensity levels of CatD immunostaining among NCI (71.1 ± 12.2), MCI (72.9 ± 12.7) and AD (68.3 ± 10.9) (p=0.69) cases.

Differential expression in PreC CatD-positive layer III neurons between MCI and NCI

Custom-designed microarray analysis revealed upregulation of 10 genes and downregulation of 9 genes out of the 576 transcripts belonging to 11 different gene oncology categories (GOCs) in PreC CatD-positive layer III neurons in MCI compared to NCI (Table 3 and Fig. 2a). Comparing MCI and NCI, we found transcript upregulation for truncated tau 6D isoform with E2 and E3 (*MAPT2N6D*; p=0.003), truncated tau 6P isoform with only E2 (*MAPT1N6P*; p=0.01), B-cell CLL/lymphoma 2 (*BCL2*; p=0.01; Fig. 3a), dynein light chain LC8-type 1 (*DNCLC1*; p=0.01), *RAB4A*, (p=0.003; Fig. 4a), beclin 1, (*BECN1*; p=0.03[t]; Fig. 4a), glutamate receptor NMDA R2C (*GRIN2C*; p=0.003), dipeptidyl-peptidase 6

(*DPP6*; p=0.02[t]), dipeptidyl-peptidase 10 (*DPP10*; p=0.004) and aminopeptidase puromycin sensitive (*PSA*; p=0.008). A comparison between MCI and NCI revealed transcript downregulation for islet amyloid polypeptide (*IAPP*; p=0.005), nestin (*NES*; p=0.005), neurofilament heavy polypeptide (*NEFH*; p=0.008), EPH receptor A2, epithelial cell protein tyrosine kinase (*EPHA2*; p=0.04[t]), glutamate receptor ionotropic kainate 5 (*GRIK5*; p=0.03[t]), cocaine- and amphetamine-regulated transcript (*CART*; p=0.04[t]), gamma-aminobutyric acid (*GABA*) A receptor, alpha 1 (*GABRA1*; p=0.01), calcium channel, voltage-dependent, N type, alpha 1B subunit (*CACNA1B*; p=0.01), and macrophage scavenger receptor 1 (*MSR1*; p=0.04[t]).

Differential expression in PreC CatD positive layer III neurons in AD compared to NCI

Custom-designed microarray analysis revealed upregulation of 49 genes and downregulation of 18 genes in PreC CatD-positive layer III neurons in AD compared to NCI (Table 4) that belonged to 18 different GOCs (Table 4, Fig 2b). Comparison between AD and NCI revealed upregulation of *BCL2* (p=0.01; Fig 3b), 3 EL and autophagy related genes {*RAB5A*(p=0.01), *RAB11A* (p=0.009;Fig. 4b) and cathepsin C (*CTSC*; p=0.05[t]}, upregulation of monoamine neurotransmission genes {choline acetyltransferase (*CHAT*; p=0.04[t]; Fig. 5), butyrylcholinesterase (*BCHE*; p=0.02[t]; Fig. 5), nicotinic cholinergic receptor alpha 2 (*CHRNA2*; p=0.03[t]; Fig. 5), alpha 4 (*CHRNA4*; p=0.02[t]; Fig 5), and alpha 5 (*CHRNA5*; p=0.02[t]), serotonin transporter (*SERT*) solute carrier family 6 member 4 (*SLC6A4*; p=0.003), noradrenaline transporter (*NET*) solute carrier family 6 member 2 (*SLC6A2*; p=0.01), dopamine receptor D2 (*DRD2*; p=0.02[t]) and D4 (*DRD4*; p=0.04[t])} and 5 glutamate receptor subunits (kainate 3 (*GRIK3*; p=0.003), NMDAR 2B (*GRIN2B*; p=0.03[t]), metabotropic glutamate receptor subunits *GBM1* (p=0.004; Fig. 6), metabotropic 2 (*GRM2*; p=0.02[t]; Fig. 6), and metabotropic 5 (*GRM5*; p=0.009; Fig. 6)}. A comparison between AD and NCI revealed upregulation of 6 cytoskeletal elements including *DNCLC1* (p=0.002), neurofilament light polypeptide (*NEFL*; p=0.0002; Fig. 7), neurofilament medium polypeptide (*NEFM*; p=0.002; Fig. 7), β-actin (*ACTB*; p=0.002; Fig. 7), microtubule-associated protein 2 (*MAP2*; p=0.008; Fig. 7), and clathrin heavy polypeptide (*CLTC*; p=0.04[t]), 4 AD-related transcripts {amyloid A4 (*SAA4*; p=0.01), nicastrin (*NCSTN*; p=0.01), high density lipoprotein binding protein (*HDLBP*; p=0.02[t]), serum amyloid P component (*APCS*; p=0.03[t])}, and select steroid-related genes {hydroxysteroid (17-beta) dehydrogenase 1(*HSD17B1*; p=0.0004; Fig. 8), nuclear receptor subfamily 5 group A member 1 (*NR5A1* also known as *SF1*; p=0.002; Fig. 8), and nuclear receptor subfamily 4 group A member 2 (*NR4A2* also known as *NURR1*; p=0.04[t])}.

Further analysis of AD and NCI demonstrated downregulation of channel-related transcripts {potassium voltage-gated channel (Kv) shaker-related subfamily member 2 (*KCNA2*; p=0.02[t]), Kv channel interacting protein 1 (*KCNIP1*; p=0.03[t]), *CACNA1B* (p=0.005)}, EL and autophagy related genes {lysosomal-associated membrane protein 1 (*LAMP1*; p=0.008), autophagy related 10 (*ATG10*; p=0.002) and palmitoyl-protein thioesterase 1 (*PPT1*; p=0.02[t])}, steroid receptor transcripts nuclear receptor corepressor 2 (*NCOR2*) (p=0.01; Fig. 8) and glucocorticoid receptor nuclear receptor subfamily 3 group C member 1 (*NR3C1*; p=0.05[t]; Fig. 8) as well as monoamine neurotransmission genes {nicotinic beta cholinergic

receptor 4 (*CHRNB4*; p=0.03[t]), dopamine receptor D3 (*DRD3*; p=0.03[t]), adrenergic receptor alpha 2A (*ADRA2A*; p=0.04[t]), and *CART* (p=0.03[t])}.

Differential expression in PreC CatD-positive layer III neurons in AD compared to MCI

Custom-designed microarray analysis revealed upregulation of 54 genes and downregulation of 14 genes in PreC CatD-positive layer III neurons, which belonged to 16 different GOCs (Table 5, Fig. 2c). Comparing AD and MCI revealed upregulation of 2 EL and autophagy pathway transcripts *RAB11A* (p=0.04[t]; Fig 4b) and myosin VB (*MYO5B*; p=0.006), upregulation of 7 cholinergic neurotransmission transcripts {*CHAT* (p=0.005; Fig. 5), *BCHE* (p=0.02[t]; Fig. 5), muscarinic cholinergic receptors *CHRM1* (p=0.03[t]) and *CHRM3* (p=0.01), nicotinic cholinergic receptors *CHRNA1* (p=0.05[t]), *CHRNA2* (p=0.02[t]; Fig. 5), and *CHRNA4* (p=0.003; Fig 5)}, 3 dopamine receptors {*DRD2* (p=0.002) and *DRD4* (p=0.02[t]), *SLC6A4* (p=0.0005)} and serotonin receptor 3A (*HTR3A*; p=0.03[t]). This comparison also revealed upregulation of 8 glutamate neurotransmission transcripts {ionotropic glutamate receptors kainate 2 (*GRIK2*; p=0.006) and NMDAR 2D (*GRIN2D*; p=0.003) and metabotropic glutamate receptors *GRM1* (p=0.003; Fig. 6), *GRM2* (p=0.007; Fig. 6), *GRM5* (p=0.01; Fig. 6), *GRM7* (p=0.03[t]), and *GRM8* (p=0.02[t]), and glial high-affinity glutamate transporter EAAT1 (solute carrier family 1 member3; *SLC1A3*; p=0.03[t])}, upregulation of 5 cytoskeletal elements {*NEFL* (p=0.0008; Fig. 7), *ACTB* (p=0.04[t]; Fig. 7), *NEFM* (p=0.01; Fig. 7), alpha tubulin 1 (*TUBA1*; p=0.05[t]) and *MAP2* (p=0.04[t]; Fig. 7)}. Comparing AD and MCI further demonstrated upregulation of 7 AD related transcripts {*APP* (p=0.003), *HDLBP* (p=0.0008), *SAA4* (p=0.004), *beta-2-microglobulin* (*B2M*; p=0.01), low density lipoprotein receptor-related protein 1 (*LRP1*; p=0.02[t]), *NCSTN* (p=0.03[t]) and epiphycan (*EPYC*) (p=0.04[t])}, and 2 steroid-related genes *HSD17B1* (p=0.002; Fig. 8) and *NR5A1*(*SF1*; p=0.006; Fig. 8).

A comparison between AD and MCI revealed downregulation of 4 channel-related transcripts {*KCNA2* (p=0.05[t]), Kv shaker-related subfamily, member 6 (*KCNA6*; p=0.04[t]), *DPP6* (p=0.03[t]), and *DPP10* (p=0.02[t])}, the EL gene *LAMP1* (p=0.005), autophagy gene *BECN1* (p=0.002), and steroid-related genes glucocorticoid receptors *NR3C1* (p=0.02[t]; Fig. 8) and *NCOR2* (p=0.02[t]; Fig. 8).

Select temporal transcript dysregulation during the progression of AD

Among the 19 differentially expressed genes found between NCI and MCI, significant upregulation of *BCL2* and *DNCLC1* transcripts occurred in MCI, ultimately resulting in significant upregulation in AD, demonstrating a clear progression. Similarly, significant downregulation of *CACNA1B* was found in MCI and AD. There was a trend for downregulation of *MSR1* in MCI, which reached significance in AD. Of the differentially expressed genes found in AD compared to NCI and MCI, 20 showed either significant or trend level upregulation, whereas 5 genes displayed significant or trend level downregulation in AD compared to NCI and MCI. From NCI to MCI, expression levels of *SAA4*, *NEFL*, *PPP3CC*, *HSD17B1*, *NR5A1*, *GRM1*, *GRM5*, *LAMP1*, and *SLC2A5* were stable. Expression levels of *SAA4*, *NEFL*, *PPP3CC*, *HSD17B1*, *NR5A1*, *GRM1*, and *GRM5* displayed significant upregulation in AD compared to NCI and MCI. Concomitantly, *LAMP1* and *SLC2A5* expression levels were significantly downregulated in AD compared

to NCI and MCI. Expression levels of *RGS9*, *BCHE*, *CHRNA2*, *NR3C1*, and *KCNA2* were unchanged from NCI to MCI. In contrast, expression levels of *RGS9*, *BCHE*, and *CHRNA2* displayed trend level upregulation whereas expression levels of *NR3C1* and *KCNA2* were downregulated in AD compared to NCI and MCI. *ACTB*, *MAP2*, *RAB11A* and *TIMP1* expression levels were similar between NCI and MCI. In contrast, *ACTB*, *MAP2*, *RAB11A* and *TIMP1* levels were significantly upregulated in AD compared to NCI and displayed trend level upregulation in AD compared to MCI. *NCOR2* expression was significantly downregulated in AD compared to NCI. There was a trend level downregulation of *NCOR2* in AD compared to MCI. Moreover, transcript levels of *HDLBP*, *GRM2*, *CHAT*, *CHRNA4*, *DRD2*, and *HOMER1* displayed significant upregulation in AD compared to MCI and trend level upregulation in AD compared to NCI. These 'step up' and 'step down' expression levels between NCI, MCI, and AD indicate we were able to discriminate temporal events of select changes for many targets during the progression of dementia within this vulnerable PreC CatD-positive layer III cell type.

qPCR validation

Since it was not practical to validate every gene, we initially chose three stably expressed genes (*GALR1*, *BAP1*, and *RBM3*) from the custom-designed microarray analysis for validation as positive controls. qPCR revealed changes in expression of *GALR1* (p=0.6), *BAP1* (p=0.4), and *RBM3* (p=0.2) similar to expression direction derived from the microarray analysis of PreC CatD-positive layer III neurons showing that no transcript differences between NCI, MCI, and AD (Table 6, Fig. 10). qPCR was also used to evaluate expression levels of *RAB11A*, *HOMER1*, *GNG2*, *GRM1*, *SLC2A5*, *TIMP1*, and *RPS6KB1*, which were differentially expressed in PreC neurons in AD compared to NCI and MCI. qPCR showed significant upregulation for *RAB11A* (p=0.01) and *HOMER1* (p=0.04) in AD compared to NCI (Table 6, Fig 9) similar to the single population microarray data. qPCR analysis found no changes in the expression of *RAB11A* (p=0.4) and *HOMER1* (p=0.63) in AD versus MCI compared to the upregulation derived from the single population microarray analysis. qPCR product expression revealed stable levels for *GNG2* (p=0.6), *SLC2A5* (p=0.6), and *RPS6KB1* (p=0.2), which did not follow the downregulation seen in the single cell microarray analysis among NCI, MCI, and AD groups. Expression of qPCR products for *GRM1* (p=0.5) and *TIMP1* (p=0.5) were stable in PreC among NCI, MCI, and AD, which is different from the upregulation of *GRM1* and *TIMP1* seen in AD compared to NCI and MCI derived from the microarray data (Table 6, Fig. 9). *CHAT* expression level was below the limit of qPCR detection, so no comparison to the single cell microarray analysis was possible.

Discussion

A custom-designed array platform of 576 genes was used to define gene expression profiles of individual PreC CatD-positive layer III neurons combined with qPCR validation of select transcripts. Because literally dozens of genes displayed dysregulation in MCI and AD, we highlighted those transcripts either upregulated or downregulated relevant towards understanding mechanisms underlying the vulnerability of this cortical cell type. For example, results showed significant upregulation of *BCL2* in MCI and AD compared to

NCI. *BCL2* inhibits apoptosis and protects neurons against cell death (Yang & Korsmeyer, 1996). Although Western blotting (Kitamura et al., 1998) and immunostaining for *BCL2* immunostaining (Satou et al., 1995) revealed increased protein in hippocampus, entorhinal and temporal cortex, respectively in AD compared to normal controls, reduced *BCL2* staining was found in neurons positive for the tau epitopes AT8 and PHF-1 (Satou et al., 1995). By contrast, we reported immunoblotting data showing an increase in *BCL2* protein in the PreC in AD compared to NCI (Perez et al., 2015). These observations together with our current findings of a significant upregulation of *BCL2* in MCI and AD suggest that PreC CatD-positive layer III neurons are exhibiting a cellular plasticity response related to cell survival during the progression of AD that may be a valuable marker for therapeutic development.

Transcript analysis revealed selective upregulation of several EL and autophagy genes including *RAB4A*, *RAB11A*, and *BECN*1. *RAB4A* regulates membrane trafficking and is associated with early endosomes and is involved in cell sorting and recycling (Mohrmann et al., 2002; van der Sluijs et al., 1992). Upregulation of *RAB4A* protein and mRNA correlates with measurements of cognitive decline in individuals with MCI and AD (Ginsberg et al., 2011). *RAB11A* is associated with recycling endosomes and regulating vesicular trafficking (Ullrich et al., 1996). *RAB11* is involved in the recycling of β-secretase to the plasma membrane and affects Aβ production (Udayar et al., 2013). Although the present study found upregulation of *BECN1* in MCI compared to NCI in PreC CatD-positive layer III neurons, others report no change of *BECN1* in CA1 pyramidal neurons in AD (Bordi et al., 2016) or downregulation of *BECN1* protein levels in midfrontal cortex of moderate to severe AD patients (Pickford et al., 2008). Together, these findings suggest cell- and region-specificity of *BECN1* gene and encoded protein regulation during the progression of dementia.

The current findings revealed a trend toward an upregulation of several cholinergic transcripts (*BCHE*, *CHAT*, *CHRNA2 and CHRNA4*) in PreC layer III Cat D positive neurons in AD compared to NCI. *CHAT* and *CHRNA4* displayed significant upregulation, whereas *BCHE* and *CHRNA2* show trend level upregulation in AD compared to MCI. However, qPCR and Nanonstring Counter (data not shown) findings failed to detect *CHAT* mRNA in the PreC. Although several studies report cortical *CHAT* protein derived from the cholinergic neurons of the nucleus basalis of Meynert (nbM) (Mufson et al., 2007), most gene expression studies have failed to detect *CHAT* mRNA in the cortex (Butcher et al., 1992; Ibáñez et al., 1991; Oh et al., 1992), which would explain the lack of expression in the present study. On the other hand, *BCHE*, a serine hydrolase that is widely distributed throughout the central nervous system and also catalyzes the hydrolysis of acetylcholine, is localized to cortical neurons and is associated with NFTs and senile plaques in the AD cortex (Wright et al., 1993; Moran et al., 1994; Gomez-Ramos & Moran, 1997), supporting the current transcript findings of this cholinoceptive marker in PreC neurons. Select nicotinic acetylcholine receptor subtypes were also found to be reduced in the AD cerebral cortex (Whitehouse et al., 1986). Prior studies revealed a significant reduction in [3H]nicotine binding sites in the putamen and nbM and a reduction of [3H]QNB binding in the nbM and hippocampus in AD (Shimohama et al., 1986). In cortex, protein activity of CHRNA4 is reduced while mRNA level remains stable in AD, suggesting a disconnect between

transcription and translation of *CHRNA4* in AD (Nordberg, 2001). High-affinity nicotine binding showed a decrease in α4/β2 nicotinic receptors in hippocampus and temporal neocortex in AD (Perry et al., 1995). The present data showing an increase PreC neuronal *BCHE*, *CHRNA2*, and *CHRNA4* transcripts support their involvement in the vulnerability of these corticocortical projection neurons.

A significant upregulation of metabotropic glutamate receptors *GRM1* and *GRM5* and trend level upregulation for *GRM2* was found in AD compared to NCI. In addition, we found significant upregulation of the metabotropic glutamate receptors *GRM1*, *GRM2* and *GRM5* in AD compared to MCI. These data suggest progressive dysregulation of several presynaptic and postsynaptic metabotropic glutamate receptors in PreC neurons. On the other hand, *GRM1* was downregulated in AD frontal cortex, which correlated with the progression of AD (Albasanz et al., 2005). Activation of *GRM1* accelerates the processing of APP into non-amyloidogenic products by α-secretase *in vitro* (Lee et al., 1995) and also initiates PI3 kinase activity preventing neuronal apoptosis (Rong et al., 2003). Similar to the PreC, *GRM2* is upregulated in the AD hippocampus and colocalizes with NFTs (Lee et al., 2009), suggesting a role in the cellular pathogenesis of this disease. Taken together, these finding suggest an interplay between a putative neuroprotective action related to *GRM1* and *GRM5* upregulation versus upregulation of *GRM2*, which may lead to PreC neuronal dysfunction early in the onset of AD.

In terms of regulating cytoskeletal elements, we observed upregulation of *NEFL*, *NEFM*, *MAP2*, and *ACTB* in AD compared to NCI. Significant upregulation of *NEFL* and *NEFM* and trend for upregulation of *MAP2* and *ACTB* were found in AD compared to MCI. Western blotting studies demonstrated hyperphosphorylation of *NEFH* and *NEFM* and a significant increase in levels of *NEFH*, *NEFM* and *NEFL* in AD neocortex (Wang et al., 2001). O-GlcNAcylation and phosphorylation of *NEFM* regulate each other in cultured neuroblastoma cells and decreased O-GlcNAcylation and increased phosphorylation of *NEFM* were reported in the medial temporal cortex in AD (Deng et al., 2008), suggesting a role for these transcripts in AD neuropathology.

The present study also showed differential regulation of several steroid-related markers including significant upregulation of *HSD17B1* and *NR5A1* and trend towards downregulation for *NR3C1* in AD compared MCI and NCI. We also observed a significant downregulation of *NCOR2* in AD compared to NCI and trend level downregulation of *NCOR2* between AD and MCI. *HSD17B1*, the enzyme catalyzing conversion of estrone to estradiol, was upregulated in the PreC similar to that seen in the prefrontal cortex in AD (Luchetti et al., 2011). In Down syndrome, a genetic model of AD, women with homozygous alleles at rs676387 (intron 4), rs605059 (exon 6), and rs598126 (exon 4) of *HSD17B1* have an increased risk of dementia (Lee et al., 2012). Set-association analysis revealed that a rare haplotype in the 5' regulatory region of the *HSD17B1* gene was a risk factor for sporadic AD (de Quervain et al., 2004). *NR5A1* (*SF1*) is a steroidogenic tissue-specific nuclear receptor that regulates nearly all genes of the glycolytic pathway. Knockdown of *NR5A1* by small interfering RNA reduces the production of ATP, nicotinamide adenine dinucleotide phosphate, and downregulates genes involved in glucose metabolism (Baba et al., 2014). *NR3C1*, a glucocorticoid receptor that regulates

glucocorticoid-responsive expression is related to cognitive impairment and neurodegeneration in rodents (Montkowski et al., 1995; Murphy et al., 2002). *NCOR2* (also known as *SMART*) is a nuclear receptor co-repressor that mediates transcriptional silencing of target genes that regulate mitochondrial oxidative metabolism and aging processes (Reilly et al., 2010). Interestingly, a repressor complex containing *NCOR2* and the epigenetic marker *HDAC1* regulates *Notch* signaling transduction pathways (Kao et al., 1998). *NCOR2* forms a stable complex with *HDAC3* and functions as an activating cofactor of this epigenetic factor. In contrast, *NCOR2* does not directly activate class II *HDACs* (Guenther et al., 2001; Fischle et al., 2002). Class II *HDACs* regulate transcription by bridging the *NCOR1/NCOR2-HDAC3* complex (Fischle et al., 2002). Together, these findings suggest that transcripts related to steroid production and regulation of their receptors are involved in gene transcription and epigenetic modulation related to the cellular pathogenesis of PreC neurons in AD.

In select cases, there was a disconnect between the findings at the single population level in the custom-designed microarray analysis and that derived from regional PreC findings determined by qPCR. This discrepancy is not uncommon due to the admixed cell types within regional tissue samples required for qPCR analysis. Similar to our previous human postmortem nbM and hippocampal microarray and qPCR analyses (Ginsberg et al., 2000, 2006a, 2006b, 2010; Counts et al., 2007, 2008, 2009), we were able to validate several transcripts, often those with moderate to high expression levels, providing clear evidence of validation. Here, we chose 5 upregulated genes (*RAB11A*, *HOMER1*, *GRM1*, *CHAT* and *TIMP1*) and 3 downregulated genes (*GNG2*, *SLC2A5* and *RPS6KB1*) for qPCR validation that were related to AD in comparison to NCI and MCI. These 8 genes belong to 7 gene ontology classes with relative higher expression levels and small p-values ($p \leq 0.01$) in at least one comparison (e.g., AD vs NCI and AD vs MCI). qPCR confirmed upregulation of *RAB11A* and *HOMER1* in AD compared to NCI verifying observations from the microarray experiments. qPCR detected unchanged levels of *GRM1*, *TIMP1*, *GNG2*, *SLC2A5*, and *RPS6KB1* in PreC among NCI, MCI and AD, which did not match our array findings. Further, the discrepancy between the present single population microarray and our inability to perform qPCR validation related to *CHAT* upregulation may be related to the fact that this gene is not highly expressed in cortical neurons, which can be overwhelmed by the complexity of gene expressions related to multiple cell types located within the cortical layers of the PreC. An alternative approach for validation of single population microarray findings is *in situ* hybridization (Ginsberg et al., 2000), which can be applied to a population of individual neurons within a well-defined cortical lamina similar to the LCM-based microarray approach used in the current study. However, *in situ* hybridization carries its own limitations and pitfalls, especially in postmortem human brain tissue. Due to a lack of available tissue samples for *in situ* hybridization, we selected the more conventional qPCR approach to validate custom-designed microarray results.

A caveat of this and other postmortem human brain tissue studies is the role that end of life agonal state exerts upon RNA expression levels in the brain. The effects of agonal conditions on nucleic acids are well documented and an average PMI of 3–4 h is considered optimal for gene expression analysis (Blair et al., 2016). Current PMIs were ~5 h which are appropriate for gene expression studies. Another consideration is that this investigation examined PreC

CatD-immunopositive neurons irrespective of NFT status. Since we did not differentiate accrued from NFT-positive or negative neurons, as done in prior studies (Tiernan et al., 2016, 2018), we were unable to attribute the effect of tau pathology on specific expression profiles during the progression of dementia. This neuronal distinction will be investigated upon access to additional precuneal sections and the maximization of double immunolabeling for LCM experiments. Another limitation is the relatively small number of APOE ε4 carriers, particularly homozygous individuals, which likely affect the associations described here. Future studies consisting of a greater balance of APOE ε4 carriers and non-carriers are needed. Moreover, the individuals in the present investigation were from a community-based group of highly educated retired clergy who were provided excellent health care and nutrition (Bennett et al., 2012; Mufson et al., 2012). Volunteer subjects may introduce bias by decreasing pathology but this, in part, is mitigated by the high follow-up and autopsy rates of the RROS cohort (Bennett et al., 2005). Strengths of the study include uniform premortem clinical and postmortem pathological evaluation and that final pathologic classification was performed without knowledge of the clinical evaluation.

In summary, PreC CatD-positive layer III neurons display significant dysregulation of anti-apoptotic, EL and autophagy genes in MCI and AD indicating early involvement of cell survival and cellular trafficking systems in the pathogenesis of these neurons. Upregulation of type I metabotropic glutamate receptor (*GRM1* and *GRM5*), type II metabotropic glutamate receptor (*GRM2*) in AD compared to NCI and MCI also suggest a role in neuronal pathogenesis. Upregulation of mRNA for the cholinoceptive marker *BCHE* and acetylcholine receptors *CHRNA2* and *CHRNA4* reveal dysregulation of cholinergic-related genes in the pathogenesis of PreC layer III neurons in AD. In addition, upregulation of cytoskeletal element transcripts (*NEFL*, *NEFM*, *MAP2*, and *ACTB*) also indicate participation in the pathogenesis of AD. Differential expression of steroid-related marker and receptors implicate involvement in gene transcription and epigenetic regulation in the cellular pathogenesis of PreC neurons in AD. Together, the present findings suggest that PreC CatD-positive layer III neurons undergo a diverse dysregulation of multiple transcripts affecting different functional pathways during the onset of AD.

Acknowledgements:

We are indebted to the nuns, priests, and lay brothers who participated in the Rush Religious Orders Study and to the members of the Rush ADC.

Funding: This study was supported by grants PO1 AG014449, RO1 AG043375, RO1 AG010161, P01 AG017617, and RO1 AG042146 from the National Institute on Aging, Barrow Neurological Institute Barrow and Beyond and the Fine Foundation.

References

Albasanz JL, Dalfo E, Ferrer I, & Martin M (2005). Impaired metabotropic glutamate receptor/phospholipase C signaling pathway in the cerebral cortex in Alzheimer's disease and dementia with Lewy bodies correlates with stage of Alzheimer's-disease-related changes. Neurobiol Dis, 20 (3), 685–693. DOI: 10.1016/j.nbd.2005.05.001 [PubMed: 15949941]

Albert M, Smith LA, Scherr PA, Taylor JO, Evans DA, & Funkenstein HH (1991). Use of brief cognitive tests to identify individuals in the community with clinically diagnosed Alzheimer's disease. Int J Neurosci, 57 (3-4), 167–178. DOI: 10.3109/00207459109150691 [PubMed: 1938160]

Alldred MJ, Che S, & Ginsberg SD (2008). Terminal Continuation (TC) RNA amplification enables expression profiling using minute RNA input obtained from mouse brain. Int J Mol Sci, 9 (11), 2091–2104. DOI: 10.3390/ijms9112091 [PubMed: 19165351]

Alldred MJ, Che S, & Ginsberg SD (2009). Terminal continuation (TC) RNA amplification without second strand synthesis. J Neurosci Methods, 177 (2), 381–385. DOI: 10.1016/j.jneumeth.2008.10.027 [PubMed: 19026688]

Alldred MJ, Chao HM, Lee SH, Beilin J, Powers BE, Petkova E, … Ginsberg SD. (2018). CA1 pyramidal neuron gene expression mosaics in the Ts65Dn murine model of Down syndrome and Alzheimer's disease following maternal choline supplementation. Hippocampus, 28 (4), 251–268. DOI: 10.1002/hipo.22832 [PubMed: 29394516]

Andrews-Hanna JR, Snyder AZ, Vincent JL, Lustig C, Head D, Raichle ME, & Buckner RL (2007). Disruption of large-scale brain systems in advanced aging. Neuron, 56 (5), 924–935. DOI: 10.1016/j.neuron.2007.10.038 [PubMed: 18054866]

Baba T, Otake H, Sato T, Miyabayashi K, Shishido Y, Wang CY … Morohashi K. (2014). Glycolytic genes are targets of the nuclear receptor Ad4BP/SF-1. Nat Commun, 5, 3634–3646. DOI: 10.1038/ncomms4634 [PubMed: 24727981]

Bennett DA, Schneider JA, Bienias JL, Evans DA, & Wilson RS (2005) Mild cognitive impairment is related to Alzheimer disease pathology and cerebral infarctions. Neurology, 64 (5), 834–841. DOI: 10.1212/01.WNL.0000152982.47274.9E [PubMed: 15753419]

Bennett DA, Schneider JA, Arvanitakis Z, Kelly JF, Aggarwal NT, Shah R , & Wilson RS (2006). Neuropathology of older persons without cognitive impairment from two community-based studies. Neurology, 66 (12), 1837–1844. DOI: 10.1212/01.wnl.0000219668.47116.e6 [PubMed: 16801647]

Bennett DA, Wilson RS, Boyle PA, Buchman AS, & Schneider JA (2012). Relation of neuropathology to cognition in persons without cognitive impairment. Ann Neurol, 72 (4), 599–609. DOI: 10.1002/ana.23654 [PubMed: 23109154]

Blair JA, Wang C, Hernandez D, Siedlak SL, Rodgers MS, Achar RK, …Lee HG. (2016). Individual Case Analysis of Postmortem Interval Time on Brain Tissue Preservation. PLoS One, 11 (3),e0151615 DOI: 10.1371/journal.pone.0151615 [PubMed: 26982086]

Bordi M, Berg MJ, Mohan PS, Peterhoff CM, Alldred MJ, Che S, … Nixon RA. (2016). Autophagy flux in CA1 neurons of Alzheimer hippocampus: Increased induction overburdens failing lysosomes to propel neuritic dystrophy. Autophagy, 12 (12),2467–2483. DOI: 10.1080/15548627.2016.1239003 [PubMed: 27813694]

Braak H, & Braak E (1991). Neuropathological stageing of Alzheimer-related changes. Acta Neuropathol, 82 (4), 239–259. DOI: 10.1007/bf00308809 [PubMed: 1759558]

Buckner RL, Andrews-Hanna JR, & Schacter DL (2008). The brain's default network: anatomy, function, and relevance to disease. Ann N Y Acad Sci, 1124, 1–38. DOI: 10.1196/annals.1440.011 [PubMed: 18400922]

Butcher LL, Oh JD, Woolf NJ, Edwards RH, & Roghani A (1992). Organization of central cholinergic neurons revealed by combined in situ hybridization histochemistry and choline-O-acetyltransferase immunocytochemistry. Neurochem Int, 21 (3), 429–445. DOI: 10.1016/0197-0186(92)90195-w [PubMed: 1303168]

Cataldo AM, Barnett JL, Berman SA, Li J, Quarless S, Bursztajn S, … Nixon RA. (1995). Gene expression and cellular content of cathepsin D in Alzheimer's disease brain: evidence for early up-regulation of the endosomal-lysosomal system. Neuron, 14 (3), 671–680. DOI: 10.1016/0896-6273(95)90324-0 [PubMed: 7695914]

Cataldo AM, Hamilton DJ, Barnett JL, Paskevich PA, & Nixon RA (1996). Properties of the endosomal-lysosomal system in the human central nervous system: disturbances mark most neurons in populations at risk to degenerate in Alzheimer's disease. J Neurosci, 16 (1), 186–199. [PubMed: 8613784]

Cataldo AM, Barnett JL, Pieroni C, & Nixon RA (1997). Increased neuronal endocytosis and protease delivery to early endosomes in sporadic Alzheimer's disease: neuropathologic evidence for a mechanism of increased beta-amyloidogenesis. J Neurosci, 17 (16),6142–6151. [PubMed: 9236226]

Che S, & Ginsberg SD (2004). Amplification of RNA transcripts using terminal continuation. Lab Invest, 84 (1), 131–137. DOI: 10.1038/labinvest.3700005 [PubMed: 14647400]

Counts SE, He B, Che S, Ikonomovic MD, DeKosky ST, Ginsberg SD, & Mufson EJ (2007). Alpha7 nicotinic receptor up-regulation in cholinergic basal forebrain neurons in Alzheimer disease. Arch Neurol, 64 (12), 1771–1776. DOI: 10.1001/archneur.64.12.1771 [PubMed: 18071042]

Counts SE, He B, Che S, Ginsberg SD, & Mufson EJ (2008). Galanin hyperinnervation upregulates choline acetyltransferase expression in cholinergic basal forebrain neurons in Alzheimer's disease. Neurodegener Dis, 5, 228–331. DOI: 10.1159/000113710 [PubMed: 18322398]

Counts SE, He B, Che S, Ginsberg SD, & Mufson EJ (2009). Galanin fiber hyperinnervation preserves neuroprotective gene expression in cholinergic basal forebrain neurons in Alzheimer's disease. J Alzheimers Dis, 18, 885–896. DOI: 10.3233/JAD-2009-1196 [PubMed: 19749437]

Davis DG, Schmitt FA, Wekstein DR, & Markesbery WR (1999). Alzheimer neuropathologic alterations in aged cognitively normal subjects. J Neuropathol Exp Neurol, 58 (4), 376–388. DOI: 10.1097/00005072-199904000-00008 [PubMed: 10218633]

de Quervain DJ, Poirier R, Wollmer MA, Grimaldi LM, Tsolaki M, Streffer JR, … Papassotiropoulos A. (2004). Glucocorticoid-related genetic susceptibility for Alzheimer's disease. Hum Mol Genet, 13 (1), 47–52. DOI: 10.1093/hmg/ddg361 [PubMed: 14583441]

Deiss LP, Galinka H, Berissi H, Cohen O, & Kimchi A (1996). Cathepsin D protease mediates programmed cell death induced by interferon-gamma, Fas/APO-1 and TNF-alpha. EMBO J, 15 (15), 3861–3870. [PubMed: 8670891]

Deng Y, Li B, Liu F, Iqbal K, Grundke-Iqbal I, Brandt R, & Gong CX (2008). Regulation between O-GlcNAcylation and phosphorylation of neurofilament-M and their dysregulation in Alzheimer disease. FASEB J, 22 (1), 138–145. DOI: 10.1096/fj.07-8309com [PubMed: 17687114]

Devanand DP, Folz M, Gorlyn M, Moeller JR, & Stern Y (1997). Questionable dementia: clinical course and predictors of outcome. J Am Geriatr Soc, 45 (3),321–328. DOI: 10.1111/j.1532-5415.1997.tb00947.x [PubMed: 9063278]

Drzezga A, Becker JA, Van Dijk KR, Sreenivasan A, Talukdar T, Sullivan C, … Sperling RA. (2011). Neuronal dysfunction and disconnection of cortical hubs in non-demented subjects with elevated amyloid burden. Brain, 134 (Pt 6), 1635–1646. DOI: 10.1093/brain/awr066 [PubMed: 21490054]

Eberwine J, & Crino P (2001). Analysis of mRNA populations from single live and fixed cells of the central nervous system. Curr Protoc Neurosci, Chapter 5: Unit 5.3. DOI: 10.1002/0471142301.ns0503s00

Ebly EM, Hogan DB, & Parhad IM (1995). Cognitive impairment in the nondemented elderly. Results from the Canadian Study of Health and Aging. Arch Neurol, 52 (6), 612–619. DOI: 10.1001/archneur.1995.00540300086018 [PubMed: 7763211]

Fischle W, Dequiedt F, Hendzel MJ, Guenther MG, Lazar MA, Voelter W, & Verdin E (2002). Enzymatic activity associated with class II HDACs is dependent on a multiprotein complex containing HDAC3 and SMRT/N-CoR. Mol Cell, 9 (1), 45–57. DOI: 10.1016/s1097-2765(01)00429-4 [PubMed: 11804585]

Flicker C, Ferris SH, & Reisberg B (1991). Mild cognitive impairment in the elderly: predictors of dementia. Neurology, 41 (7), 1006–1009. DOI: 10.1212/wnl.41.7.1006 [PubMed: 2067629]

Frisoni GB, Testa C, Sabattoli F, Beltramello A, Soininen H, & Laakso MP (2005). Structural correlates of early and late onset Alzheimer's disease: voxel based morphometric study. J Neurol Neurosurg Psychiatry, 76 (1), 112–114. DOI: 10.1136/jnnp.2003.029876 [PubMed: 15608008]

Ginsberg SD, Hemby SE, Lee VM, Eberwine JH, & Trojanowski JQ (2000). Expression profile of transcripts in Alzheimer's disease tangle-bearing CA1 neurons. Ann Neurol, 48 (1), 77–87. [PubMed: 10894219]

Ginsberg SD, & Che S (2005). Expression profile analysis within the human hippocampus: comparison of CA1 and CA3 pyramidal neurons. J Comp Neurol, 487(1), 107–118. DOI: 10.1002/cne.20535 [PubMed: 15861457]

Ginsberg SD, Che S, Counts SE, & Mufson EJ (2006a) Single cell gene expression profiling in Alzheimer's disease. NeuroRx,3 (3), 302–318. DOI: 10.1016/j.nurx.2006.05.007 [PubMed: 16815214]

Ginsberg SD, Che S, Counts SE, & Mufson EJ. (2006b). Shift in the ratio of three-repeat tau and four-repeat tau mRNAs in individual cholinergic basal forebrain neurons in mild cognitive impairment and Alzheimer's disease. J Neurochem, 96 (5), 1401–1408. DOI: 10.1111/j.1471-4159.2005.03641.x [PubMed: 16478530]

Ginsberg SD (2008). Transcriptional profiling of small samples in the central nervous system. Methods Mol Biol, 439, 147–158. DOI: 10.1007/978-1-59745-188-8_10 [PubMed: 18370101]

Ginsberg SD, Alldred MJ, Counts SE, Cataldo AM, Neve RL, Jiang Y, … Che S. (2010). Microarray analysis of hippocampal CA1 neurons implicates early endosomal dysfunction during Alzheimer's disease progression. Biol Psychiatry, 68 (10), 885–893. DOI: 10.1016/j.biopsych.2010.05.030 [PubMed: 20655510]

Ginsberg SD, Mufson EJ, Alldred MJ, Counts SE, Wuu J, Nixon RA, & Che S (2011). Upregulation of select rab GTPases in cholinergic basal forebrain neurons in mild cognitive impairment and Alzheimer's disease. J Chem Neuroanat, 42 (2),102–110. DOI: 10.1016/j.jchemneu.2011.05.012 [PubMed: 21669283]

Ginsberg SD, Malek-Ahmadi MH, Alldred MJ, Che S, Elarova I, Chen Y, … Mufson EJ. (2019). Selective decline of neurotrophin and neurotrophin receptor genes within CA1 pyramidal neurons and hippocampus proper: Correlation with cognitive performance and neuropathology in mild cognitive impairment and Alzheimer's disease. Hippocampus, 29 (5), 422–439. DOI: 10.1002/hipo.22802 [PubMed: 28888073]

Gómez-Ramos P, & Morán MA (1997). Ultrastructural localization of butyrylcholinesterase in senile plaques in the brains of aged and Alzheimer disease patients. Mol Chem Neuropathol, 30 (3), 161–173. DOI: 10.1007/bf02815095 [PubMed: 9165483]

Guenther MG, Barak O, & Lazar MA (2001). The SMRT and N-CoR corepressors are activating cofactors for histone deacetylase 3. Mol Cell Biol, 21 (18), 6091–6101. DOI: 10.1128/mcb.21.18.6091-6101.2001 [PubMed: 11509652]

Herholz K, Salmon E, Perani D, Baron JC, Holthoff V, Frölich L, … Heiss W. (2002). Discrimination between Alzheimer dementia and controls by automated analysis of multicenter FDG PET. Neuroimage, 17 (1), 302–316. DOI: 10.1006/nimg.2002.1208 [PubMed: 12482085]

Ibáñez CF, Ernfors P, & Persson H (1991). Developmental and regional expression of choline acetyltransferase mRNA in the rat central nervous system. J Neurosci Res, 29 (2),163–171. DOI: 10.1002/jnr.490290205 [PubMed: 1890697]

Ishii K, Kawachi T, Sasaki H, Kono AK, Fukuda T, Kojima Y, & Mori E (2005). Voxel-based morphometric comparison between early- and late-onset mild Alzheimer's disease and assessment of diagnostic performance of z score images. AJNR Am J Neuroradiol, 26 (2), 333–340. [PubMed: 15709131]

Josephs KA, Murray ME, Whitwell JL, Tosakulwong N, Weigand SD, Petrucelli L, … Dickson DW. (2016). Updated TDP-43 in Alzheimer's disease staging scheme. Acta Neuropathol, 131(4), 571–585. DOI: 10.1007/s00401-016-1537-1 [PubMed: 26810071]

Kao HY, Ordentlich P, Koyano-Nakagawa N, Tang Z, Downes M, Kintner CR, … Kadesch T. (1998). A histone deacetylase corepressor complex regulates the Notch signal transduction pathway. Genes Dev, 12 (15), 2269–2277. DOI: 10.1101/gad.12.15.2269 [PubMed: 9694793]

Karas G, Scheltens P, Rombouts S, van Schijndel R, Klein M, Jones B, … Barkhof F. (2007). Precuneus atrophy in early-onset Alzheimer's disease: a morphometric structural MRI study. Neuroradiology, 49 (12),967–976. DOI: 10.1007/s00234-007-0269-2 [PubMed: 17955233]

Khurana V, Elson-Schwab I, Fulga TA, Sharp KA, Loewen CA, Mulkearns E, … Feany MB (2010). Lysosomal dysfunction promotes cleavage and neurotoxicity of tau in vivo. PLoS Genet, 6 (7), e1001026 DOI: 10.1371/journal.pgen.1001026 [PubMed: 20664788]

Kitamura Y, Shimohama S, Kamoshima W, Ota T, Matsuoka Y, Nomura Y, … Taniguchi T. (1998). Alteration of proteins regulating apoptosis, Bcl-2, Bcl-x, Bax, Bak, Bad, ICH-1 and CPP32, in Alzheimer's disease. Brain Research, 780 (2),260–269. DOI: 10.1016/s0006-8993(97)01202-x [PubMed: 9507158]

Lee HG, Zhu X, Casadesus G, Pallas M, Camins A, O'Neill MJ, … Smith MA. (2009). The effect of mGluR2 activation on signal transduction pathways and neuronal cell survival. Brain Res, 1249, 244–250. DOI: 10.1016/j.brainres.2008.10.055 [PubMed: 19026996]

Lee JH, Gurney S, Pang D, Temkin A, Park N, Janicki SC, … Schupf N. (2012). Polymorphisms in HSD17B1: Early Onset and Increased Risk of Alzheimer's Disease in Women with Down Syndrome. Curr Gerontol Geriatr Res, 2012, 361218 DOI: 10.1155/2012/361218 [PubMed: 22474448]

Lee RK, Wurtman RJ, Cox AJ, & Nitsch RM (1995). Amyloid precursor protein processing is stimulated by metabotropic glutamate receptors. Proc Natl Acad Sci U S A, 92 (17), 8083–8087. DOI: 10.1073/pnas.92.17.8083 [PubMed: 7644542]

Luchetti S, Bossers K, Van de Bilt S, Agrapart V, Morales RR, Frajese GV, & Swaab DF (2011). Neurosteroid biosynthetic pathways changes in prefrontal cortex in Alzheimer's disease. Neurobiol Aging, 32 (11), 1964–1976. DOI: 10.1016/j.neurobiolaging.2009.12.014 [PubMed: 20045216]

Matsuda H (2007). The role of neuroimaging in mild cognitive impairment. Neuropathology, 27: 570–577. DOI: 10.1111/j.1440-1789.2007.00794.x [PubMed: 18021379]

McKhann G, Drachman D, Folstein M, Katzman R, Price D, & Stadlan EM (1984). Clinical diagnosis of Alzheimer's disease: report of the NINCDS-ADRDA Work Group under the auspices of Department of Health and Human Services Task Force on Alzheimer's Disease. Neurology, 34 (7), 939–944. DOI: 10.1212/wnl.34.7.939 [PubMed: 6610841]

Mintun MA, Larossa GN, Sheline YI, Dence CS, Lee SY, Mach RH, … Morris JC. (2006). [11C]PIB in a nondemented population: potential antecedent marker of Alzheimer disease. Neurology, 67 (3), 446–452. DOI: 10.1212/01.wnl.0000228230.26044.a4 [PubMed: 16894106]

Mirra SS (1997). The CERAD neuropathology protocol and consensus recommendations for the postmortem diagnosis of Alzheimer's disease: a commentary. Neurobiol Aging, 18 (4 Suppl), S91–94. DOI: 10.1016/s0197-4580(97)00058-4 [PubMed: 9330994]

Mohrmann K, Gerez L, Oorschot V, Klumperman J, & van der Sluijs P (2002). Rab4 function in membrane recycling from early endosomes depends on a membrane to cytoplasm cycle. J Biol Chem, 277 (35), 32029–32035. DOI: 10.1074/jbc.M203064200 [PubMed: 12036958]

Montkowski A, Barden N, Wotjak C, Stec I, Ganster J, Meaney M, … Holsboer, (1995). Long-term antidepressant treatment reduces behavioural deficits in transgenic mice with impaired glucocorticoid receptor function. J Neuroendocrinol, 7 (11), 841–845. DOI: 10.1111/j.1365-2826.1995.tb00724.x [PubMed: 8748120]

Morán MA, Mufson EJ, & Gomez-Ramos P (1994). Cholinesterases colocalize with sites of neurofibrillary degeneration in aged and Alzheimer's brains. Acta Neuropathol, 87 (3), 284–292. DOI: 10.1007/bf00296744 [PubMed: 8009960]

Mufson EJ, Lavine N, Jaffar S, Kordower JH, Quirion R, & Saragovi HU (1997). Reduction in p140-TrkA receptor protein within the nucleus basalis and cortex in Alzheimer's disease. Exp Neurol, 146 (1), 91–103. DOI: 10.1006/exnr.1997.6504 [PubMed: 9225742]

Mufson EJ, Chen EY, Cochran EJ, Beckett LA, Bennett DA, & Kordower JH (1999). Entorhinal cortex beta-amyloid load in individuals with mild cognitive impairment. Exp Neurol, 158 (2), 469–490. DOI: 10.1006/exnr.1999.7086 [PubMed: 10415154]

Mufson EJ, Counts SE, Fahnestock M, & Ginsberg SD (2007). Cholinotrophic molecular substrates of mild cognitive impairment in the elderly. Curr Alzheimer Res, 4 (4), 340–350. DOI: 10.2174/156720507781788855 [PubMed: 17908035]

Mufson EJ, Binder L, Counts SE, DeKosky ST, de Toledo-Morrell L, Ginsberg SD, … Scheff SW. (2012). Mild cognitive impairment: pathology and mechanisms. Acta Neuropathol, 123 (1), 13–30. DOI: 10.1007/s00401-011-0884-1 [PubMed: 22101321]

Murphy EK, Spencer RL, Sipe KJ, & Herman JP (2002). Decrements in nuclear glucocorticoid receptor (GR) protein levels and DNA binding in aged rat hippocampus. Endocrinology, 143 (4), 1362–1370. DOI: 10.1210/endo.143.4.8740 [PubMed: 11897693]

Nelson PT, Abner EL, Scheff SW, Schmitt FA, Kryscio RJ, Jicha GA, … Markesbery WR. (2009). Alzheimer's-type neuropathology in the precuneus is not increased relative to other areas of neocortex across a range of cognitive impairment. Neurosci Lett, 450 (3), 336–339. DOI: 10.1016/j.neulet.2008.11.006 [PubMed: 19010392]

Newell KL, Hyman BT, Growdon JH, & Hedley-Whyte ET (1999). Application of the National Institute on Aging (NIA)-Reagan Institute criteria for the neuropathological diagnosis of

Alzheimer disease. J Neuropathol Exp Neurol, 58 (11), 1147–1155. DOI: 10.1097/00005072-199911000-00004 [PubMed: 10560657]

Nixon RA (2007). Autophagy, amyloidogenesis and Alzheimer disease. J Cell Sci, 120 (Pt 23), 4081–4091. DOI: 10.1242/jcs.019265 [PubMed: 18032783]

Nixon RA (2017). Amyloid precursor protein and endosomal-lysosomal dysfunction in Alzheimer's disease: inseparable partners in a multifactorial disease. FASEB J, 31, 2729–2743. DOI: 10.1096/fj.201700359 [PubMed: 28663518]

Nordberg A (2001). Nicotinic receptor abnormalities of Alzheimer's disease: therapeutic implications. Biol Psychiatry, 49 (3), 200–210. DOI: 10.1016/s0006-3223(00)01125-2 [PubMed: 11230871]

Oh JD, Woolf NJ, Roghani A, Edwards RH, & Butcher LL (1992). Cholinergic neurons in the rat central nervous system demonstrated by in situ hybridization of choline acetyltransferase mRNA. Neuroscience, 47 (4), 807–822. DOI: 10.1016/0306-4522(92)90031-v [PubMed: 1579211]

Pasternak SH, Callahan JW, & Mahuran DJ (2004). The role of the endosomal/lysosomal system in amyloid-beta production and the pathophysiology of Alzheimer's disease: reexamining the spatial paradox from a lysosomal perspective. J Alzheimers Dis, 6 (1), 53–65. DOI: 10.3233/jad-2004-6107 [PubMed: 15004328]

Perez SE, Getova DP, He B, Counts SE, Geula C, Desire L, … Mufson EJ. (2012). Rac1b increases with progressive tau pathology within cholinergic nucleus basalis neurons in Alzheimer's disease. Am J Pathol, 180 (2), 526–540. DOI: 10.1016/j.ajpath.2011.10.027 [PubMed: 22142809]

Perez SE, He B, Nadeem M, Wuu J, Scheff SW, Abrahamson EE, … Mufson EJ. (2015). Resilience of precuneus neurotrophic signaling pathways despite amyloid pathology in prodromal Alzheimer's disease. Biol Psychiatry, 77 (8), 693–703. DOI: 10.1016/j.biopsych.2013.12.016 [PubMed: 24529280]

Perry EK, Morris CM, Court JA, Cheng A, Fairbairn AF, McKeith IG, … Perry RH. (1995). Alteration in nicotine binding sites in Parkinson's disease, Lewy body dementia and Alzheimer's disease: possible index of early neuropathology. Neuroscience, 64 (2), 385–395. DOI: 10.1016/0306-4522(94)00410-7 [PubMed: 7700528]

Petersen RC, Smith GE, Ivnik RJ, Tangalos EG, Schaid DJ, Thibodeau SN, … Kurland LT. (1995). Apolipoprotein E status as a predictor of the development of Alzheimer's disease in memory-impaired individuals. JAMA, 273 (16), 1274–1278. [PubMed: 7646655]

Pickford F, Masliah E, Britschgi M, Lucin K, Narasimhan R, Jaeger PA, … Wyss-Coray T. (2008). The autophagy-related protein beclin 1 shows reduced expression in early Alzheimer disease and regulates amyloid beta accumulation in mice. J Clin Invest, 118 (6), 2190–2199. DOI: 10.1172/JCI33585 [PubMed: 18497889]

Raichle ME, MacLeod AM, Snyder AZ, Powers WJ, Gusnard DA, & Shulman GL (2001). A default mode of brain function. Proc Natl Acad Sci U S A, 98 (2), 676–682. DOI: 10.1073/pnas.98.2.676 [PubMed: 11209064]

Reilly SM, Bhargava P, Liu S, Gangl MR, Gorgun C, Nofsinger RR, … Lee CH. (2010). Nuclear receptor corepressor SMRT regulates mitochondrial oxidative metabolism and mediates aging-related metabolic deterioration. Cell Metab, 12 (6), 643–653. DOI: 10.1016/j.cmet.2010.11.007 [PubMed: 21109196]

Riemenschneider M, Blennow K, Wagenpfeil S, Andreasen N, Prince JA, Laws SM, … Kurz A. (2006). The cathepsin D rs17571 polymorphism: effects on CSF tau concentrations in Alzheimer disease. Hum Mutat, 27 (6), 532–537. DOI: 10.1002/humu.20326 [PubMed: 16652347]

Rombouts SA, Barkhof F, Goekoop R, Stam CJ, & Scheltens P (2005). Altered resting state networks in mild cognitive impairment and mild Alzheimer's disease: an fMRI study. Hum Brain Mapp, 26 (4), 231–239. DOI: 10.1002/hbm.20160 [PubMed: 15954139]

Rong R, Ahn JY, Huang H, Nagata E, Kalman D, Kapp JA, … Ye K. (2003). PI3 kinase enhancer-Homer complex couples mGluRI to PI3 kinase, preventing neuronal apoptosis. Nat Neurosci, 6 (11), 1153–1161. DOI: 10.1038/nn1134 [PubMed: 14528310]

Rubin EH, Morris JC, Grant EA, & Vendegna T (1989). Very mild senile dementia of the Alzheimer type. I. Clinical assessment. Arch Neurol, 46 (4), 379–382. [PubMed: 2650663]

SAS Institute Inc. SAS/STAT 9.1 User's Guide. (2004). SAS Publishing; Cary, NC.

Satou T, Cummingsa BJ, & Cotmana CW (1995). Immunoreactivity for Bcl-2 protein within neurons in the Alzheimer's disease brain increases with disease severity. Brain Res, 697 (1–2), 35–43. DOI: 10.1016/0006-8993(95)00748-f [PubMed: 8593592]

Scheff SW, Price DA, Schmitt FA, Roberts KN, Ikonomovic MD, & Mufson EJ (2013). Synapse stability in the precuneus early in the progression of Alzheimer's disease. J Alzheimers Dis, 35 (3), 599–609. DOI: 10.3233/JAD-122353 [PubMed: 23478309]

Schmitt FA, Davis DG, Wekstein DR, Smith CD, Ashford JW, & Markesbery WR (2000). "preclinical" AD revisited: neuropathology of cognitively normal older adults. Neurology, 55 (3), 370–376. DOI: 10.1212/wnl.55.3.370 [PubMed: 10932270]

Schmitt FA, Nelson PT, Abner E, Scheff S, Jicha GA, Smith C, … Kryscio RJ. (2012). University of Kentucky Sanders-Brown healthy brain aging volunteers: donor characteristics, procedures and neuropathology. Curr Alzheimer Res, 9 (6), 724–733 DOI: 10.2174/156720512801322591 [PubMed: 22471862]

Schmittgen TD, & Livak KJ (2008). Analyzing real-time PCR data by the comparative C(T) method. Nat Protoc, 3 (6), 1101–1108. DOI: 10.1038/nprot.2008.73 [PubMed: 18546601]

Sheline YI, Raichle ME, Snyder AZ, Morris JC, Head D, Wang S, & Mintun MA (2010). Amyloid plaques disrupt resting state default mode network connectivity in cognitively normal elderly. Biol Psychiatry, 67 (6), 584–587. DOI: 10.1016/j.biopsych.2009.08.024 [PubMed: 19833321]

Shimohama S, Taniguchi T, Fujiwara M, & Kameyama, (1986). M. Changes in nicotinic and muscarinic cholinergic receptors in Alzheimer-type dementia. J Neurochem, 46(1), 288–293. DOI: 10.1111/j.1471-4159.1986.tb12960.x [PubMed: 3940287]

Sperling RA, Laviolette PS, O'Keefe K, O'Brien J, Rentz DM, Pihlajamaki M , … Johnson KA. (2009). Amyloid deposition is associated with impaired default network function in older persons without dementia. Neuron, 63 (2), 178–188. DOI: 10.1016/j.neuron.2009.07.003 [PubMed: 19640477]

Sperling RA, Dickerson BC, Pihlajamaki M, Vannini P, LaViolette PS, Vitolo OV, … Johnson KA. (2010). Functional alterations in memory networks in early Alzheimer's disease. Neuromolecular Med, 12 (1), 27–43. DOI: 10.1007/s12017-009-8109-7 [PubMed: 20069392]

Tiernan CT, Ginsberg SD, Guillozet-Bongaarts AL, Ward SM, He B, Kanaan NM, … Counts SE. (2016). Protein homeostasis gene dysregulation in pretangle-bearing nucleus basalis neurons during the progression of Alzheimer's disease. Neurobiol Aging, 42, 80–90. DOI: 10.1016/j.neurobiolaging.2016.02.031 [PubMed: 27143424]

Tiernan CT, Ginsberg SD, He B, Ward SM, Guillozet-Bongaarts AL, Kanaan NM, … Counts SE. (2018). Pretangle pathology within cholinergic nucleus basalis neurons coincides with neurotrophic and neurotransmitter receptor gene dysregulation during the progression of Alzheimer's disease. Neurobiol Dis, 117, 125–136. DOI: 10.1016/j.nbd.2018.05.021 [PubMed: 29859871]

Udayar V, Buggia-Prevot V, Guerreiro RL, Siegel G, Rambabu N, Soohoo AL, … Rajendran L. (2013). A paired RNAi and RabGAP overexpression screen identifies Rab11 as a regulator of beta-amyloid production. Cell Rep, 5 (6), 1536–1551. DOI: 10.1016/j.celrep.2013.12.005 [PubMed: 24373285]

Ullrich O, Reinsch S, Urbe S, Zerial M, & Parton RG (1996). Rab11 regulates recycling through the pericentriolar recycling endosome. J Cell Biol, 135 (4), 913–924. DOI: 10.1083/jcb.135.4.913 [PubMed: 8922376]

van der Sluijs P, Hull M, Webster P, Mâle P, Goud B, & Mellman I (1992). The small GTP-binding protein rab4 controls an early sorting event on the endocytic pathway. Cell, 70 (5), 729–740. DOI: 10.1016/0092-8674(92)90307-x [PubMed: 1516131]

Wagner AD, Shannon BJ, Kahn I, & Buckner RL (2005). Parietal lobe contributions to episodic memory retrieval. Trends Cogn Sci, 9 (9), 445–453. DOI: 10.1016/j.tics.2005.07.001 [PubMed: 16054861]

Wang J, Tung YC, Wang Y, Li XT, Iqbal K, & Grundke-Iqbal I (2001). Hyperphosphorylation and accumulation of neurofilament proteins in Alzheimer disease brain and in okadaic acid-treated SY5Y cells. FEBS Lett, 507 (1), 81–87. DOI: 10.1016/s0014-5793(01)02944-1 [PubMed: 11682063]

Whitehouse PJ, Martino AM, Antuono PG, Lowenstein PR, Coyle JT, Price DL, & Kellar KJ (1986). Nicotinic acetylcholine binding sites in Alzheimer's disease. Brain Res, 371(1), 146–151. DOI: 10.1016/0006-8993(86)90819-x [PubMed: 3708340]

Wright CI, Geula C, & Mesulam MM (1993). Neurological cholinesterases in the normal brain and in Alzheimer's disease: relationship to plaques, tangles, and patterns of selective vulnerability. Ann Neurol, 34 (3), 373–384. DOI: 10.1002/ana.410340312 [PubMed: 8363355]

Yan H, Zhang Y, Chen H, Wang Y, & Liu Y (2013). Altered effective connectivity of the default mode network in resting-state amnestic type mild cognitive impairment. J Int Neuropsychol Soc, 19 (4), 400–409. DOI: 10.1017/S1355617712001580 [PubMed: 23425569]

Yang E, & Korsmeyer SJ (1996). Molecular thanatopsis: a discourse on the BCL2 family and cell death. Blood, 88 (2), 386–401. [PubMed: 8695785]

Precuneus (PreC) layer III projection neurons, which contain lysosomal hydrolase cathepsin D (CatD) are dysfunctional in Alzheimer's disease (AD). Expression profiling of CatD positive PreC layer III neurons revealed significant dysregulation of a mosaic of genes in tissue from subjects with mild cognitive impairment and AD that was not previously appreciated in terms of their indication of systems-wide signaling defects in a key hub of the default mode memory network.

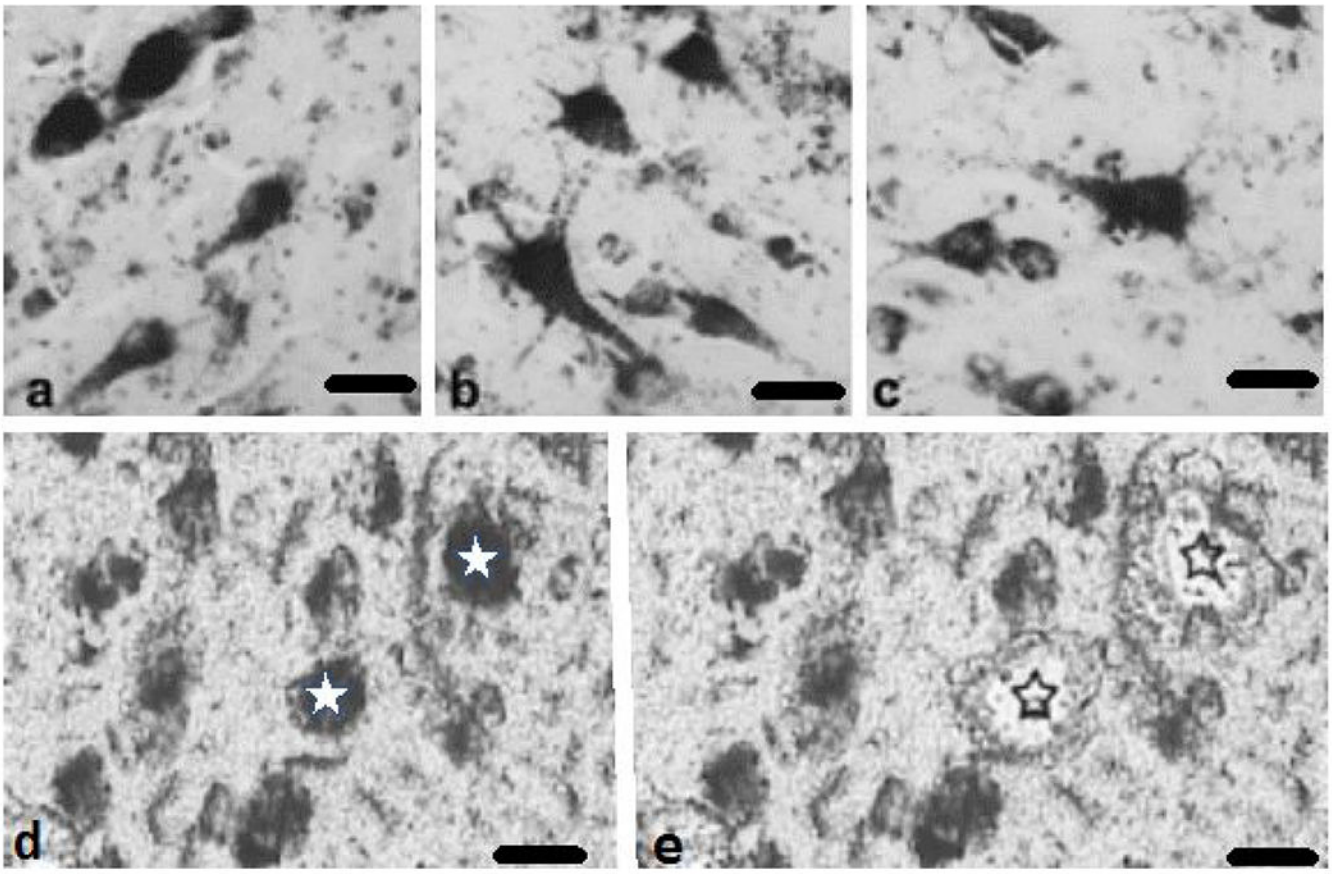

Fig. 1.

Photomicrographs showing PreC CatD-positive layer III neurons in NCI (a), MCI (b), and AD (c). CatD immunolabeled neurons pre (d, white stars) and post (e, black outlines stars) microdissection from a non-cognitively impaired 84-year old female. Distorted appearance of the images (d and e) is due to the fact that the pictures were taken from uncover slipped sections with the aid of a Zeiss PALM III LCM.. Scale bars = 25 μm

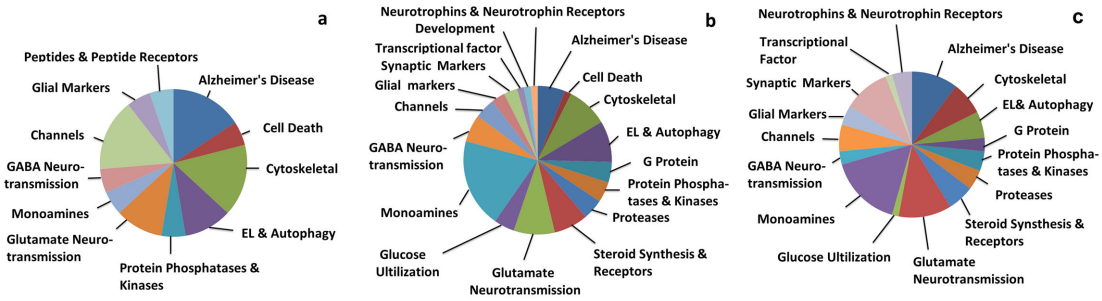

Fig. 2.

Pie charts showing gene ontology categories (GOCs) of differentially expressed genes in PreC CatD-positive layer III neurons across clinical groups, **a:** GOCs of differentially expressed genes in PreC CatD-positive layer III neurons of MCI compared to NCI; **b:** GOCs of differentially expressed genes in PreC CatD-positive layer III neurons in AD compared to NCI; **c:** GOCs of differentially expressed genes in PreC CatD-positive layer III neurons in AD compared to MCI.

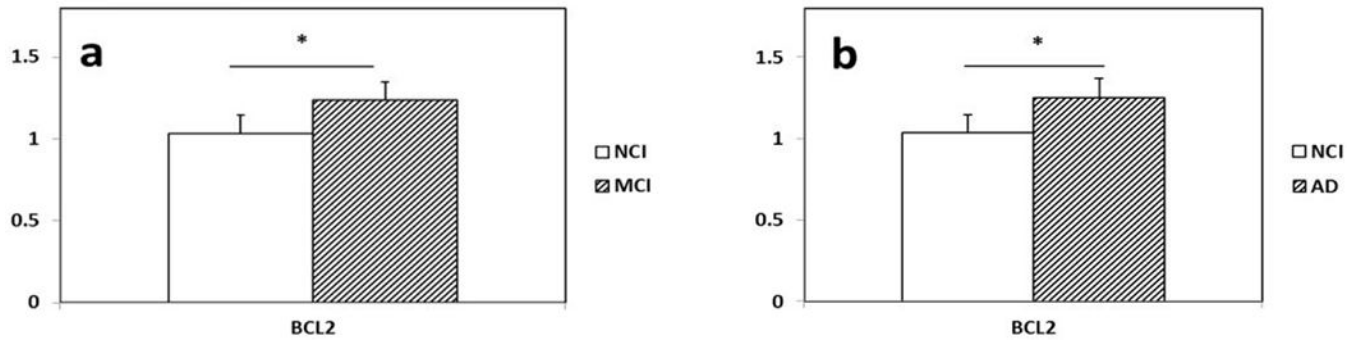

Fig. 3.

Histograms showing upregulation of *BCL2* in PreC CatD-positive layer III neurons in MCI (a) and AD (b) compared to NCI.

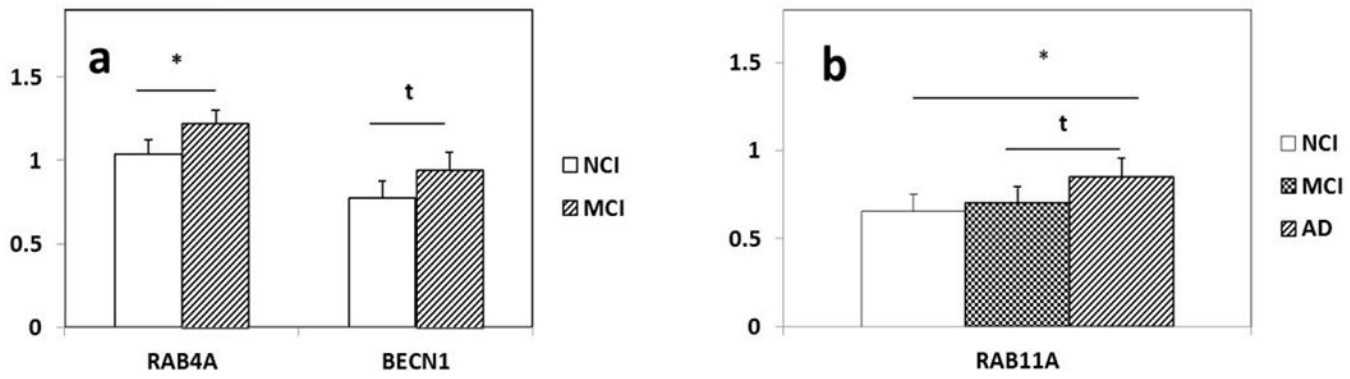

Fig. 4.

Differentially expressed endosomal lysosomal (EL) and autophagy transcripts in PreC CatD-positive layer III neurons in MCI and AD. **a:** Significant upregulation of *RAB4A* (p=0.003) and upregulation trend of *BECN1* (p=0.03^{t}) in MCI compared to NCI. **b:** Upregulation of *RAB11A* in AD compared to NCI (p=0.009) and upregulation trend of *RAB11a* (p=0.04^{t}) in AD compared to MCI. Key: $^{t\text{-trend}}$; 0.01<P<0.05; *: P⩽0.01.

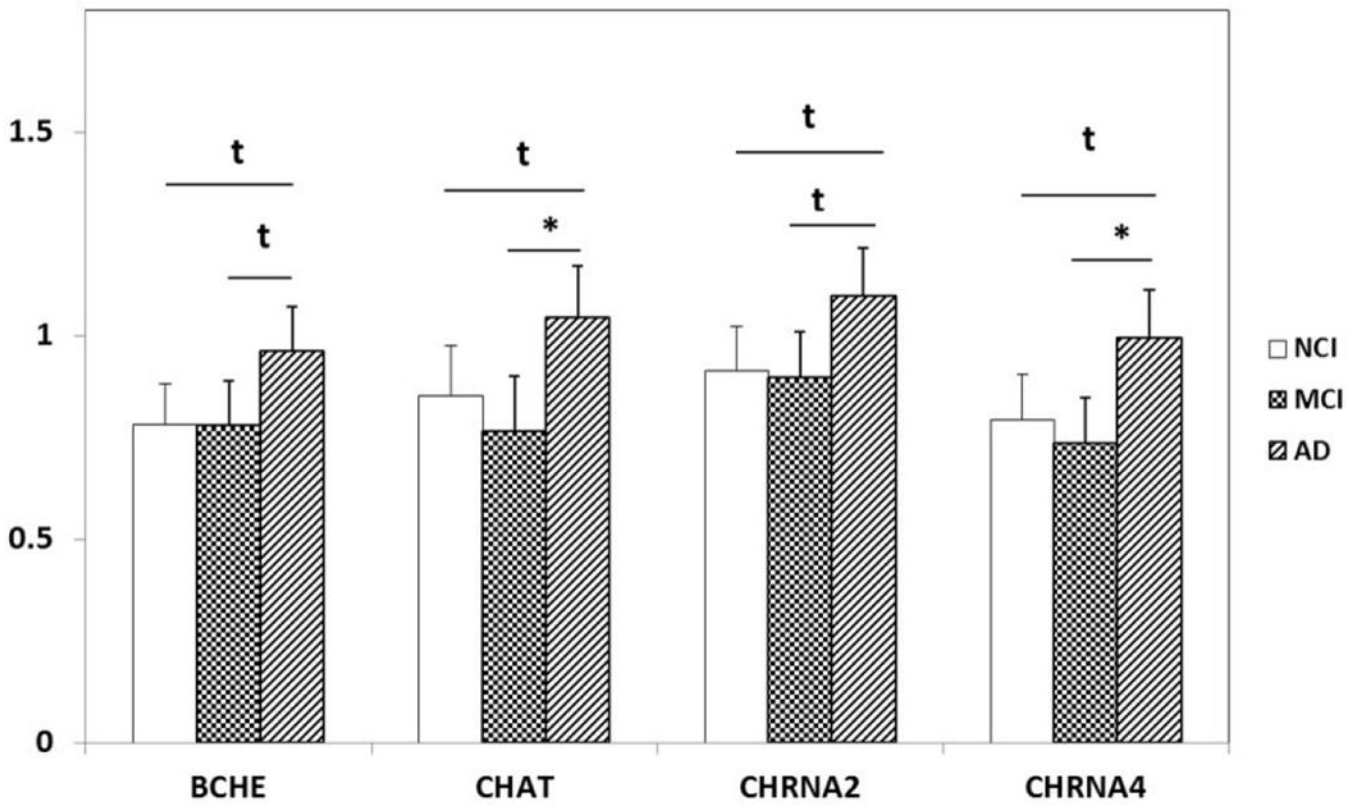

Fig. 5.

Differential expression of cholinergic enzymes (*BCHE* and *CHAT*) and nicotinic acetylcholine receptors (*CHRNA2* and *CHRNA4*) in PreC CatD-positive layer III neurons in AD compared to NCI and MCI. Upregulation trend of *BCHE* (AD>NCI, p=0.2^{t}; AD>MCI, p=0.02^{t}) and *CHRNA2* (AD>NCI, p=0.03^{t}; AD>MCI, p=0.02^{t}) in AD compared to NCI and MCI. Upregulation trend of *CHAT* (AD>NCI, p=0.04^{t}) and *CHRNA4* (AD>NCI, p=0.02^{t}) in AD compared to NCI and significant upregulation of *CHAT*(AD>MCI, p=0.005) and *CHRNA4* (AD>MCI, p=0.003) in AD compared to MCI. Key: $^{t\text{-trend}}$: 0.01<p<0.05; *: p⩽0.01.

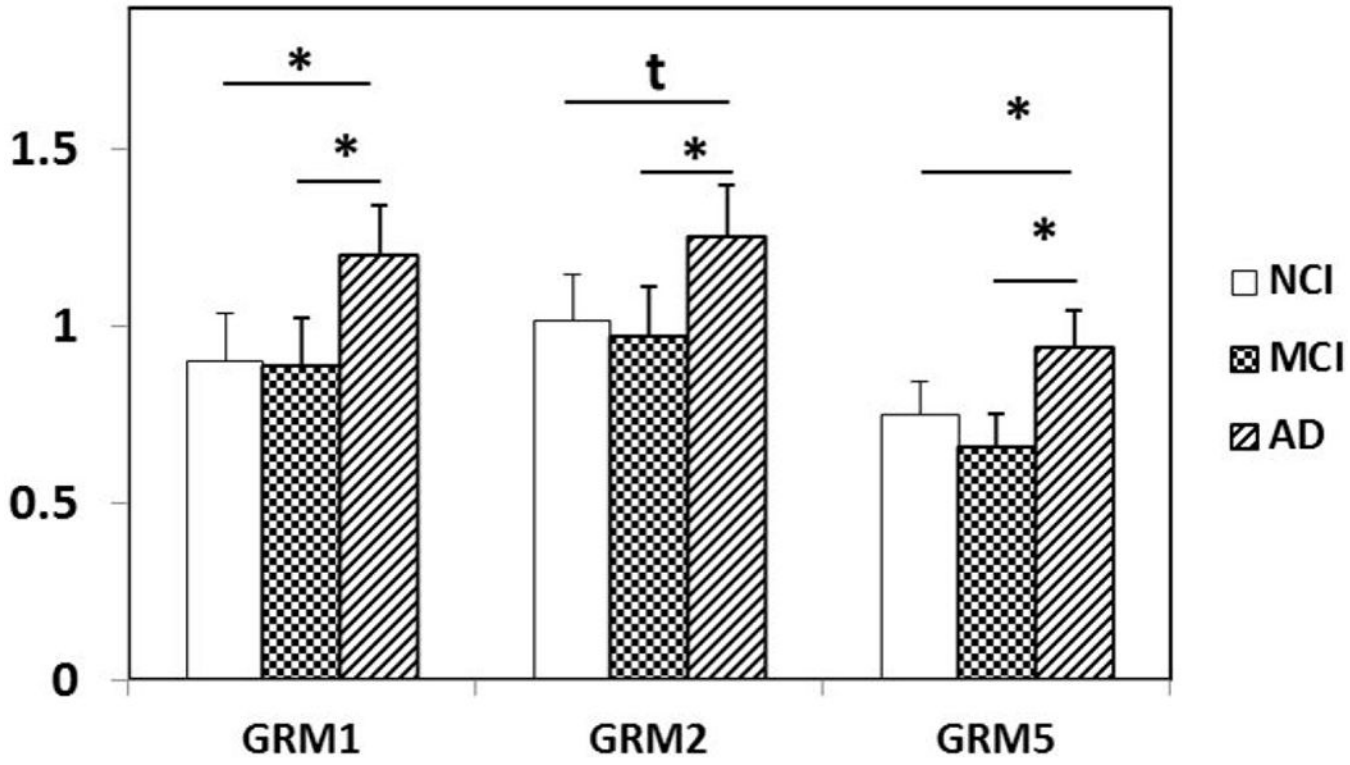

Fig. 6.

Differential expression of *GRM1*, *GRM2*, and *GRM5* in PreC CatD-positive layer III neurons in AD compared to NCI and MCI. *GRM1* (AD>NCI, p=0.004; AD>MCI, p=0.003) and *GRM5* (AD>NCI, p=0.009; AD>MCI, p=0.01) are upregulated in AD compared to NCI and MCI. Upregulation trend of *GRM2* (AD>NCI, $p=0.02^{t}$) in AD compared to NCI and significant upregulation of *GRM2* (AD>MCI, p=0.007) in AD compared to MCI. Key: $^{t\text{-trend}}$: 0.01<p<0.05; *: p≤0.01.

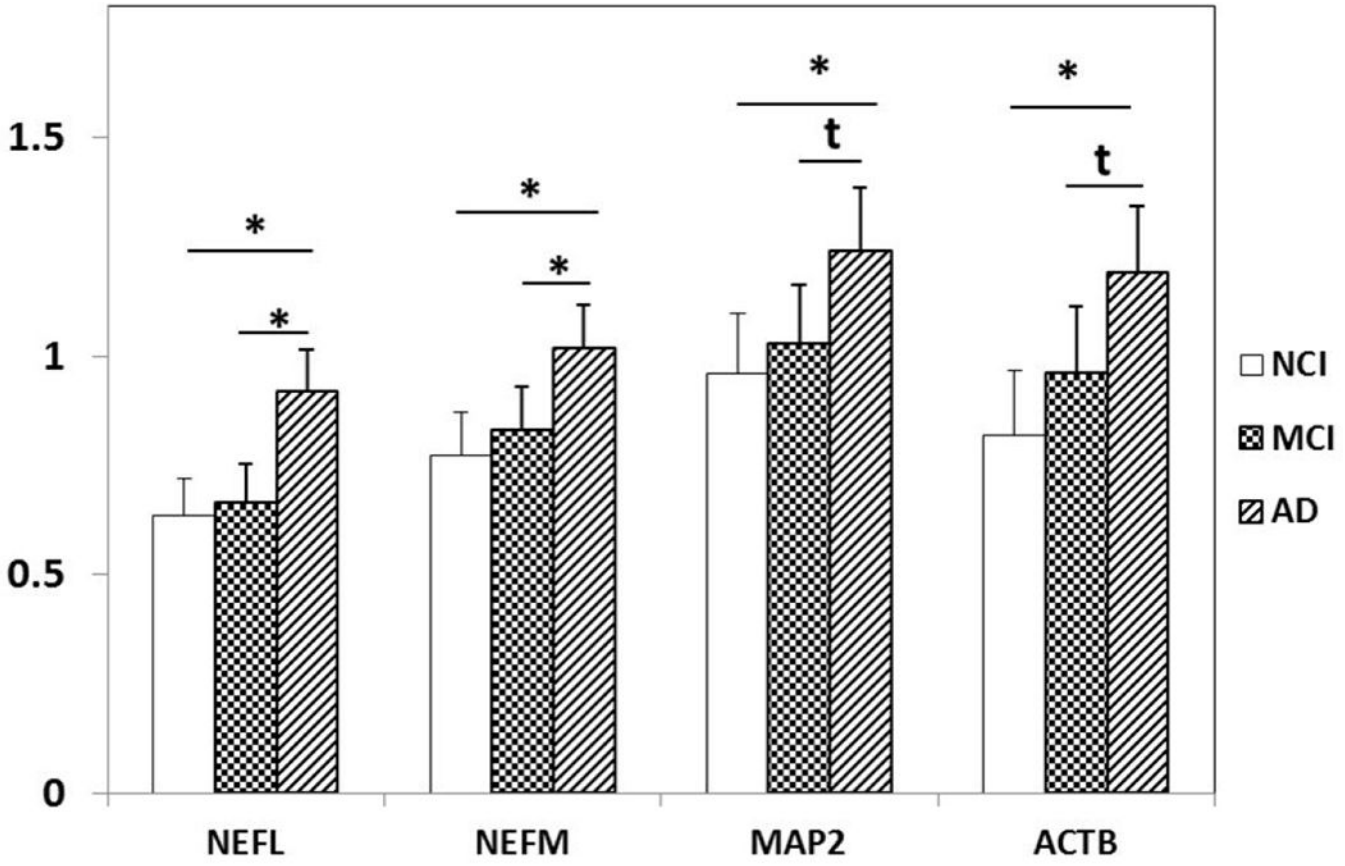

Fig. 7.

Upregulation of cytoskeletal elements *NEFL NEFM*, *MAP2* and *ACTB* in PreC CatD-positive layer III neurons in AD compared to NCI and MCI. *NEFL* (p=0.0002), *NEFM* (p=0.002), *MAP2* (p=0.008) and *ACTB* (p=0.002) are significantly upregulated in AD compared to NCI. Significant upregulation of NEFL (p=0.0008) and NEFM (p=0.01) and upregulation trend for MAP2 ($p=0.04^{t}$) and ACTB ($p=0.04^{t}$) in AD compared to MCI. Key: $^{t\text{-trend}}$: $0.01<p<0.05$, *: $p\leq 0.01$.

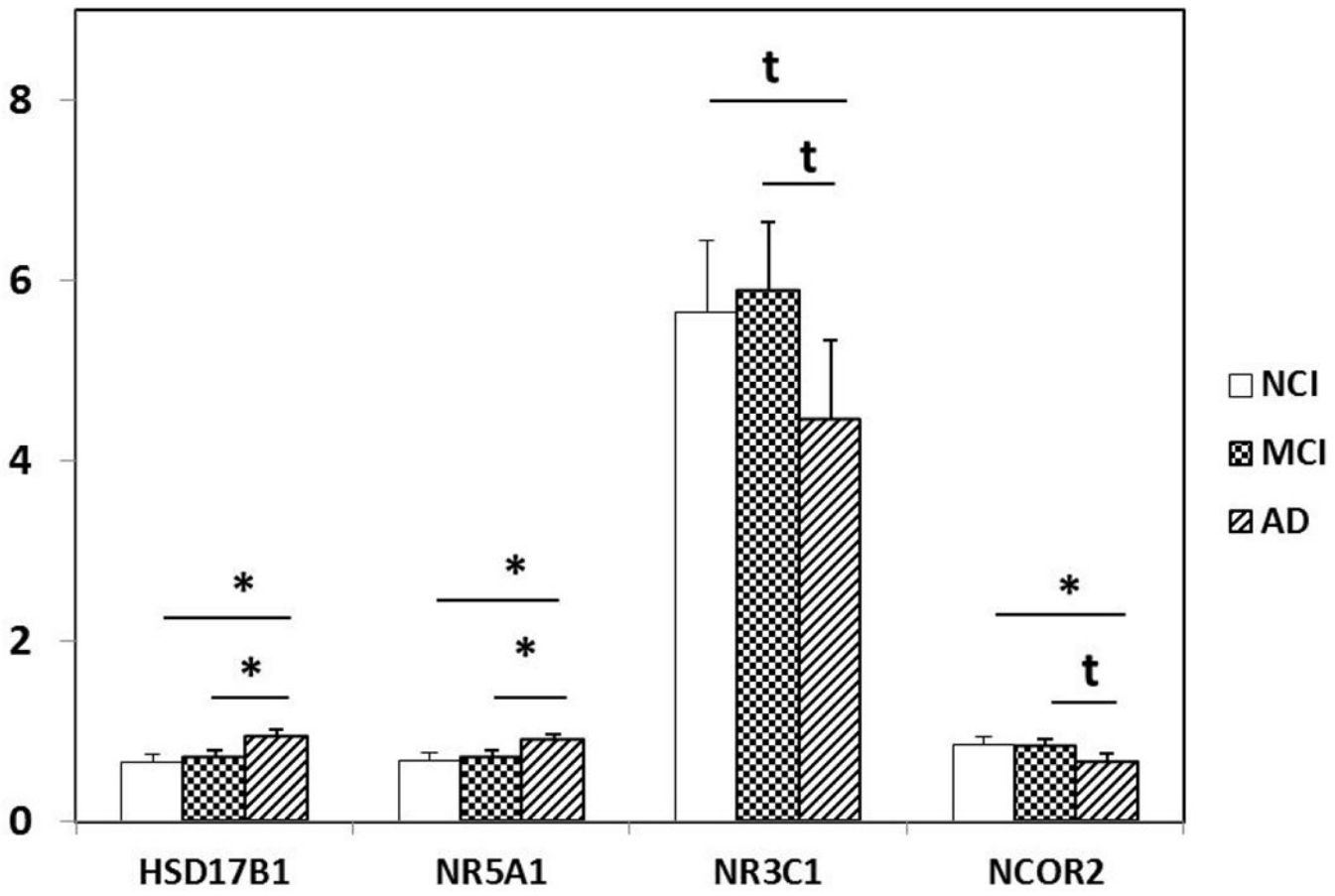

Fig 8.

Differentially expressed *HSD17B1*, *NR5A1*, *NR3C1* and *NCOR2* in PreC CatD-positive layer III neurons in AD compared to NCI and MCI. *HSD17B1* (AD>NCI, p=0.0004; AD>MCI, p=0.002) and *NR5A1* (AD>NCI, p=0.002; AD>MCI, p=0.006) are significantly upregulated in PreC CatD-positive layer III neurons in AD compared to NCI and MCI. Downregulation trend for *NR3C1* (AD<NCI, $p=0.046^{t}$; AD<MCI, $p=0.02^{t}$) in AD compared to NCI and MCI. Significant downregulation of *NCOR2* (AD<NCI, p=0.01) in AD compared to NCI and downregulation trend of NCOR2 (AD<MCI, $p=0.02^{t}$) in AD compared to MCI. Key: t-trend: $0.01<p<0.05$, *: $p\leq0.01$.

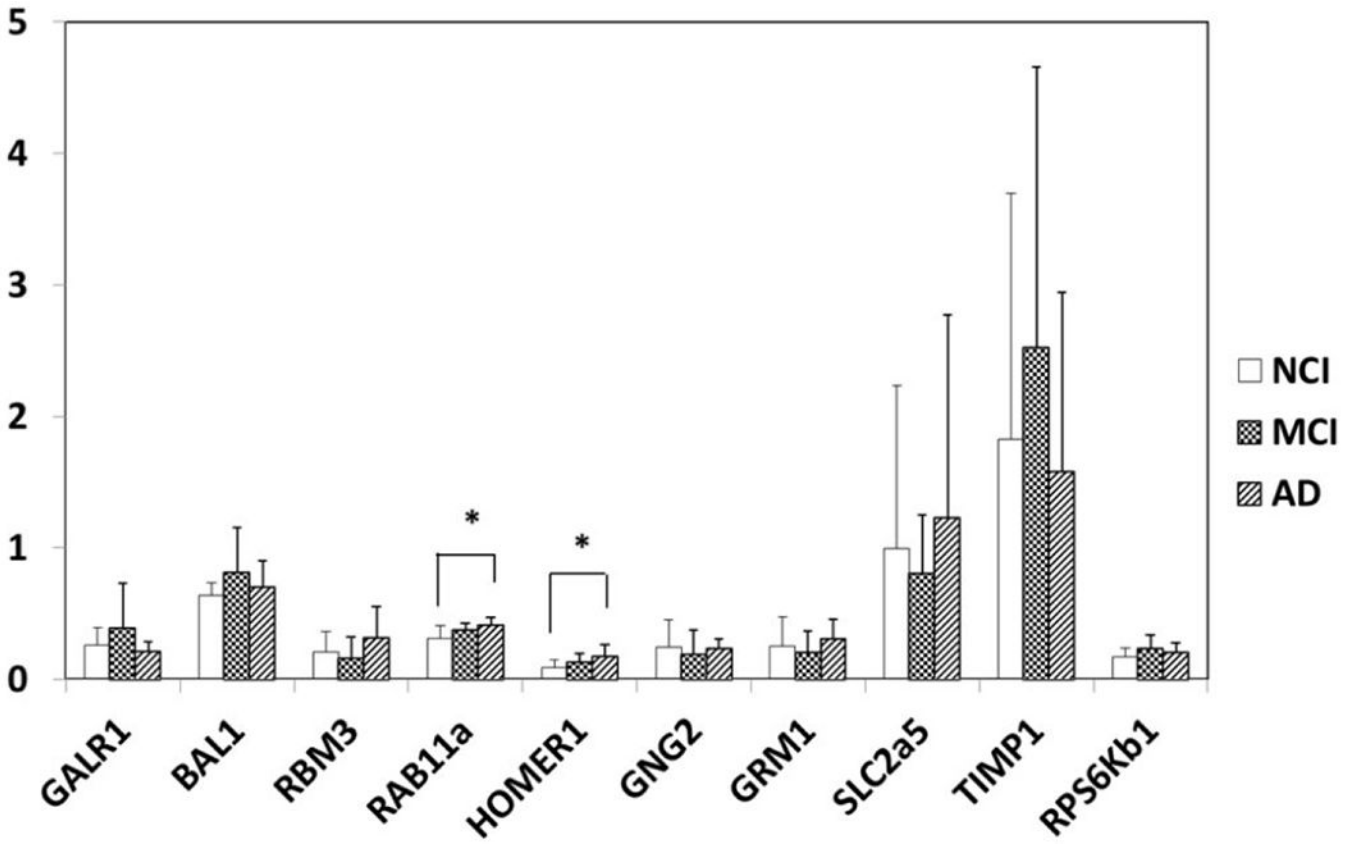

Fig. 9.

qPCR of select genes in the PreC of NCI, MCI and AD. Upregulation of *RAB11A* (p=0.02) and *HOMER1* (p=0.045) in AD compared to NCI and unchanged mRNA levels of *GALR1* (p=0.64), *BAP1* (p=0.43) and *RBM3* (p=0.2) validating microarray observations. *GNG2* (p=0.6), *GRM1* (p=0.5), *SLC2A5* (p=0.6), *TIMP1* (p=0.5) and *RPS6KB1* (p=0.2) are unchanged among NCI, MCI and AD. *: $p<0.05$.

Table 1.

Clinical and Neuropathological Case Characteristics

		NCI (N=11)	MCI (N=11)	AD (N=9)	Overall p-value	Pair-wise comparisons
Age (years) at death	Mean ± SD	86.17 ± 4.95	87.36 ± 4.58	88.48 ± 5.36	0.59	-----
Number of males (%)		3 (27)	18 (33)	3 (33)	0.74	-----
Years of education	Mean ± SD	16.91 ± 3.65	18.36 ± 2.80	18.22 ± 4.02	0.57	-----
Number with ApoE ε4 allele (%)		0 (0)	5 (45)	2 (22)	0.04	-----
MMSE	Mean ± SD	28.00 ± 1.55	26.91 ± 2.91	20.33 ± 2.43	<0.001	**NCI, MCI > AD**
GCS	Mean ± SD	−0.16 ± 0.25	−0.41 ± 0.44	−1.27 ± 0.68	<0.001	**NCI, MCI > AD**
Episodic memory z-score	Mean ± SD	0.23 ± 0.45	−0.33 ± 0.65	−1.68 ± 1.15	<0.001	**NCI, MCI > AD**
Semantic memory z-score	Mean ± SD	−0.42 ± 0.65	−0.37 ± 0.71	−0.74 ± 0.77	0.46	-----
Working memory z-score	Mean ± SD	−0.18 ± 0.49	−0.19 ± 0.69	−0.58 ± 0.59	0.25	-----
Perceptual speed z-score	Mean ± SD	−0.71 ± 0.66	−0.84 ± 0.59	−2.40 ± 0.72	<0.001	**NCI, MCI > AD**
Visuospatial z-score	Mean ± SD	−0.41 ± 0.53	−0.80 ± 0.63	−1.12 ± 0.89	0.08	----
Post-mortem interval (hours)	Mean ± SD	5.38 ± 2.11	5.44 ± 2.18	4.14 ± 1.43	0.27	-----
Brain weight (g)	Mean ± SD	1166.91 ± 86.22	1154.27 ± 141.18	1150.56 ± 88.26	0.83	-----
Distribution of Braak scores	0	0	0	0	0.76	-----
	I/II	2	2	1		
	III/IV	8	5	6		
	V/VI	1	4	2		
NIA Reagan (likelihood of AD)	No AD	0	0	0	0.17	-----
	Low	6	3	1		
	Intermediate	5	5	6		
	High	0	3	2		
CERAD	No AD	2	2	0	0.10	-----
	Possible	6	6	6		
	Probable	3	0	0		
	Definite	0	3	3		

Table 2.

qPCR TaqMan probes

Gene	Assay ID
GALR1	Hs00175668_m1
BAP1	Hs01109276_g1
RBM3	00943160_g1
RAB11A	Hs00366449_g1
HOMER1	01029333_m1
GNG2	Hs00828232_m1
GRM1	Hs00168250_m1
SLC2A5	01086390_m1
TIMP1	Hs01092512_g1
RPS6KB1	Hs00356367_m1
GAPDH	Hs02758991_g1
CHAT	Hs00758143_m1

Table 3.

Differentially expressed transcripts in PreC CatD-positive layer III neurons in MCI compared to NCI

Gene	Gene Ontology Category Group	Gene Full Name	p	FDR	MCI
MAPT2N6D	AD	truncated tau 6D isoform with E2 and E3	0.003	0.305	↑
IAPP	AD	islet amyloid polypeptide alias amylin	0.005	0.305	↓
MAPT1N6P	AD	truncated tau 6P isoform with only E2	0.01	0.452	↑
BCL2	CD	B-cell CLL/lymphoma 2	0.01	0.452	↑
NES	CYT	nestin	0.005	0.305	↓
NEFH	CYT	neurofilament, heavy polypeptide	0.008	0.452	↓
DNCLC1	CYT	dynein light chain LC8-type 1	0.01	0.452	↑
RAB4A	EALS	RAB4A, member RAS oncogene family	0.003	0.305	↑
BECN1	EALS	beclin 1, autophagy related	0.03^{t}	0.468	↑
EPHA2	PP/K	EPH receptor A2; epithelial cell protein tyrosine kinase	0.04^{t}	0.594	↓
GR1K5	GLUR	glutamate receptor ionotropic kainate 5	0.03^{t}	0.468	↓
GR1N2C	GLUR	glutamate receptor, ionotropic NMDA 2C	0.003	0.305	↑
CART	MONO	cocaine- and amphetamine-regulated transcript	0.04^{t}	0.594	↓
GABRA1	GABA	gamma-aminobutyric acid (GABA) A receptor, alpha 1	0.01	0.452	↓
CACNA1B	CH	calcium channel, voltage-dependent, N type, alpha 1B subunit	0.01	0.452	↓
DPP6	CH	dipeptidyl-peptidase 6	0.02^{t}	0.468	↑
DPP10	CH	dipeptidyl-peptidase 10	0.004	0.305	↑
MSR1	GLIA	macrophage scavenger receptor 1	0.04^{t}	0.594	↓
PSA	PEP	aminopeptidase puromycin sensitive	0.008	0.452	↑

^{t}: trend level change.

Table 4.

Differentially expressed transcripts in PreC CatD-positive layer III neurons in AD compared to NCI

Gene	Gene Oncology Category Group	Gene Full name	p	FDR	AD
SAA4	AD	serum amyloid A4	0.01	0.211	↑
NCSTN	AD	nicastrin	0.01	0.211	↑
HDLBP	AD	high density lipoprotein binding protein	0.02[t]	0.351	↑
APCS	AD	amyloid P component, serum	0.03[t]	0.351	↑
BCL2	CD	B-cell CLL/lymphoma 2	0.01	0.211	↑
NEFL	CYT	neurofilament, light polypeptide	0.0002	0.035	↑
NEFM	CYT	neurofilament, medium polypeptide	0.002	0.073	↑
ACTB	CYT	β-actin	0.002	0.073	↑
DNCLC1	CYT	dynein light chain LC8-type 1	0.002	0.096	↑
MAP2	CYT	microtubule-associated protein 2	0.008	0.211	↑
CLTC	CYT	clathrin, heavy polypeptide (He)	0.04[t]	0.357	↑
RAB11A	EALS	RAB11 A, member RAS oncogene family	0.009	0.211	↑
LAMP1	EALS	lysosomal-associated membrane protein 1	0.008	0.211	↓
ATG10	EALS	autophagy related 10	0.002	0.073	↓
CTSC	EALS	cathepsin C	0.046[t]	0.357	↑
RAB5A	EALS	RAB5A, member RAS oncogene family	0.01	0.211	↑
PPT1	EALS	palmitoyl-protein thioesterase 1	0.02[t]	0.351	↓
GNG2	GP	guanine nucleotide binding protein (G protein), gamma 2	0.0008	0.073	↓
RGS9	GP	regulator of G-protein signaling 9	0.04[t]	0.357	↑
RGS13	GP	regulator of G-protein signaling 13	0.04[t]	0.357	↑
PPP3CC	PP/K	protein phosphatase 3, catalytic subunit, gamma isoform	0.0003	0.052	↑
RPS6KB1	PP/K	ribosomal protein S6 kinase, 70kDa, polypeptide 1	0.01	0.211	↓
PRKCE	PP/K	protein kinase C, epsilon	0.02[t]	0.211	↑
TIMP1	PROT	tissue inhibitor of metalloproteinase 1	0.009	0.211	↑
GLRX	PROT	glutaredoxin (thioltransferase)	0.04[t]	0.351	↑
CAST	PROT	calpastatin	0.04[t]	0.357	↑
HSD17B1	ST	hydroxysteroid (17-beta) dehydrogenase 1	0.0004	0.073	↑
NR5A1/SF1	ST	nuclear receptor subfamily 5, group A, member 1	0.002	0.073	↑
NCOR2	ST	nuclear receptor corepressor 2	0.01	0.211	↓
NR4A2	ST	nuclear receptor subfamily 4, group A, member 2 alias NURR1	0.04[t]	0.357	↑
NR3C1	ST	nuclear receptor subfamily 3, group C, member 1 (glucocorticoid receptor)	0.046[t]	0.357	↓
GRIK3	GLUR	glutamate receptor ionotropic kainate 3	0.003	0.096	↑

Gene	Gene Oncology Category Group	Gene Full name	p	FDR	AD
GRM1	GLUR	glutamate receptor, metabotropic 1	0.004	0.211	↑
GRM2	GLUR	glutamate receptor, metabotropic 2	0.02[t]	0.211	↑
GRM5	GLUR	glutamate receptor, metabotropic 5	0.009	0.211	↑
GRIN2B	GLUR	glutamate receptor, ionotropic NMDA 2B	0.03[t]	0.351	↑
GRIA1	GLUR	glutamate receptor ionotropic AMPA 1	0.045[t]	0.357	↓
SLC2A4	GLUC	solute carrier family 2 (glucose transporter), member 4	0.02[t]	0.211	↑
SLC2A5	GLUC	solute carrier family 2 (glucose transporter), member 5	0.002	0.073	↓
SLC2A3	GLUC	solute carrier family 2 (glucose transporter), member 3	0.001	0.073	↑
SLC6A4/SERT	MONO	solute carrier family 6 (neurotransmitter transporter, serotonin), member 4,	0.003	0.211	↑
SLC6A2/NET	MONO	solute carrier family 6 (neurotransmitter transporter, noradrenalin), member 2	0.01	0.211	↑
CHRNB4	MONO	cholinergic receptor, nicotinic, beta 4	0.03[t]	0.351	↓
DRD3	MONO	dopamine receptor D3	0.03[t]	0.351	↓
CART	MONO	cocaine- and amphetamine-regulated transcript	0.03[t]	0.351	↓
DRD4	MONO	dopamine receptor D4	0.04[t]	0.351	↑
ADRA2A	MONO	adrenergic receptor, alpha 2a	0.04[t]	0.351	↓
CHAT	MONO	choline acetyltransferase	0.04[t]	0.351	↑
CHRNA2	MONO	cholinergic receptor, nicotinic, alpha2	0.03[t]	0.351	↑
BCHE	MONO	butyrylcholinesterase	0.02[t]	0.211	↑
CHRNA5	MONO	cholinergic receptor, nicotinic, alpha5	0.02[t]	0.211	↑
DRD2	MONO	dopamine receptor D2	0.02[t]	0.211	↑
CHRNA4	MONO	cholinergic receptor, nicotinic, alpha4	0.02[t]	0.211	↑
GABRA1	GABA	gamma-aminobutyric acid (GABA) A receptor, alpha 1	0.02[t]	0.211	↓
GABRG3	GABA	gamma-aminobutyric acid (GABA) A receptor, gamma 3	0.03[t]	0.351	↑
GABRA4	GABA	gamma-aminobutyric acid (GABA) A receptor, alpha 4	0.006	0.211	↑
GABBR1	GABA	gamma-aminobutyric acid (GABA) B receptor, 1	0.02[t]	0.211	↑
KCNIP1	CH	Kv channel interacting protein 1	0.03[t]	0.351	↓
KCNA2	CH	potassium voltage-gated channel, shaker-related subfamily, member 2	0.02[t]	0.211	↓
CACNA1B	CH	calcium channel, voltage-dependent, N type, alpha 1B subunit	0.005	0.211	↓
MSR1	GLIA	macrophage scavenger receptor 1	3.40E-06	0.035	↓
CSF1	GLIA	colony stimulating factor 1 (macrophage)	0.02[t]	0.351	↑
HOMER1	SYN	homer homolog 1	0.03[t]	0.351	↑

Gene	Gene Oncology Category Group	Gene Full name	p	FDR	AD
SNCB	SYN	synuclein, beta	0.049[t]	0.357	↑
ERCC1	TF	excision repair cross-complementing rodent repair deficiency, complementation group 1	0.0002	0.035	↑
DAB1	DV	disabled 1	0.04[t]	0.351	↑
IGF2R	NT	insulin-like growth factor 2 receptor	0.04[t]	0.357	↑

[t]: trend level change

Table 5.

Differentially expressed transcripts in PreC CatD-positive layer III neurons in AD compared to MCI

Gene	Gene Oncology Category Group	Gene Full name	p	FDR	AD
HDLBP	AD	high density lipoprotein binding protein	0.0008	0.122	↑
APP	AD	amyloid beta (A4) precursor protein	0.003	0.137	↑
SAA4	AD	serum amyloid A4	0.004	0.137	↑
B2M	AD	beta-2-microglobulin	0.01	0.181	↑
LRP1	AD	low density lipoprotein receptor-related protein 1 alias A2MR	0.02[t]	0.230	↑
NCSTN	AD	nicastrin	0.03[t]	0.233	↑
EPYC/	AD	epiphycan	0.04[t]	0.233	↑
NEFL	CYT	neurofilament, light polypeptide	0.0008	0.069	↑
ACTB	CYT	β-actin	0.04[t]	0.233	↑
NEFM	CYT	neurofilament, medium polypeptide	0.01	0.181	↑
TUBA1	CYT	tubulin, alpha 1	0.0499[t]	0.283	↑
MAP2	CYT	microtubule-associated protein 2	0.04[t]	0.233	↑
MYO5B	EALS	myosin VB	0.006	0.137	↑
RAB11A	EALS	RAB11 A, member RAS oncogene family	0.04[t]	0.233	↑
BECN1	EALS	beclin 1, autophagy related	0.002	0.122	↓
LAMP1	EALS	lysosomal-associated membrane protein 1	0.005	0.137	↓
RGS9	GP	regulator of G-protein signaling 9	0.03[t]	0.233	↑
GNG2	GP	guanine nucleotide binding protein (G protein), gamma 2	0.01	0.181	↓
PPP3CC	PP/K	protein phosphatase 3, catalytic subunit, gamma isoform	0.009	0.181	↑
RPS6KB1	PP/K	ribosomal protein S6 kinase, 70kDa, polypeptide 1	0.01	0.181	↓
PPP2CA	PP/K	protein phosphatase 2 (formerly 2A), catalytic subunit, alpha isoform	0.02[t]	0.230	↓
SOD1	PROT	superoxide dismutase 1	0.02[t]	0.181	↑
SOD2	PROT	superoxide dismutase 2	0.02[t]	0.181	↑
TIMP1	PROT	tissue inhibitor of metalloproteinase 1	0.04[t]	0.233	↑
HSD17B1	ST	hydroxysteroid (17-beta) dehydrogenase 1	0.002	0.122	↑
NR5A1/SF1	ST	nuclear receptor subfamily 5, group A, member 1	0.006	0.137	↑
NR3C1	ST	nuclear receptor subfamily 3, group C, member 1 (glucocorticoid receptor)	0.02[t]	0.181	↓
NCOR2	ST	nuclear receptor corepressor 2	0.02[t]	0.230	↓
GRM1	GLUR	glutamate receptor, metabotropic 1	0.003	0.122	↑
GRM2	GLUR	glutamate receptor, metabotropic 2	0.007	0.149	↑
GRM5	GLUR	glutamate receptor, metabotropic 5	0.01	0.181	↑

Gene	Gene Oncology Category Group	Gene Full name	p	FDR	AD
GRM7	GLUR	glutamate receptor, metabotropic 7	0.03[t]	0.233	↑
GRM8	GLUR	glutamate receptor, metabotropic 8	0.02[t]	0.181	↑
GRIK2	GLUR	glutamate receptor ionotropic kainate 2	0.006	0.137	↑
GRIN2D	GLUR	glutamate receptor, ionotropic NMDA 2D	0.003	0.122	↑
SLC1A3/EAAT1	GLUR	solute carrier family 1 (glial high-affinity glutamate transporter), member 3	0.03[t]	0.233	↑
SLC2A5	GLUC	solute carrier family 2 (facilitated glucose transporter), member 5	0.004	0.137	↓
BCHE	MONO	butyrylcholinesterase	0.02[t]	0.230	↑
CHAT	MONO	choline acetyltransferase	0.005	0.137	↑
SLC6A4/SERT	MONO	solute carrier family 6 (neurotransmitter transporter, serotonin), member 4,	0.0005	0.069	↑
CHRM1	MONO	cholinergic receptor, muscarinic 1	0.03[t]	0.233	↑
CHRM3	MONO	cholinergic receptor, muscarinic 3	0.01	0.181	↑
CHRNA1	MONO	cholinergic receptor, nicotinic, alphal	0.046[t]	0.283	↑
CHRNA2	MONO	cholinergic receptor, nicotinic, alpha2	0.02[t]	0.181	↑
CHRNA4	MONO	cholinergic receptor, nicotinic, alpha4	0.003	0.137	↑
DRD2	MONO	dopamine receptor D2	0.002	0.1221	↑
DRD4	MONO	dopamine receptor D4	0.02[t]	0.181	↑
HTR3A	MONO	5-hydroxytryptamine (serotonin) receptor 3A	0.03[t]	0.233	↑
SLC6A11/GAT4	GABA	solute carrier family 6 (neurotransmitter transporter, GABA), member 11	0.03[t]	0.233	↑
SLC6A13/GAT3	GABA	solute carrier family 6 (neurotransmitter transporter, GABA), member 13	0.04[t]	0.283	↑
KCNA2	CH	potassium voltage-gated channel, shaker-related subfamily, member 2	0.049[t]	0.283	↓
KCNA6	CH	potassium voltage-gated channel, shaker-related subfamily, member 6	0.04[t]	0.233	↓
DPP6	CH	dipeptidyl-peptidase 6	0.03[t]	0.233	↓
DPP10	CH	dipeptidyl-peptidase 10	0.02[t]	0.181	↓
HSP90AA1	GLIA	heat shock protein 90kDa alpha (cytosolic), class A member 1	0.02[t]	0.181	↑
DNAJA1	GLIA	DnaJ (Hsp40) homolog, subfamily A, member 1 alias HDJ2	0.03[t]	0.233	↑
MSR1	GLIA	macrophage scavenger receptor 1	0.0001	0.052	↓
ERBB2IP	SYN	erbb2 interacting protein densin-180	0.006	0.137	↑
DLG3	SYN	discs, large homolog 3 synapse-associated protein 102	0.008	0.181	↑
HOMER1	SYN	homer homolog 1	0.01	0.181	↑
SNCAIP	SYN	synuclein, alpha interacting protein (synphilin)	0.01	0.181	↑
SAP47	SYN	synapse-associated protein 47kD	0.02[t]	0.181	↑
SNCG	SYN	synuclein, gamma	0.04[t]	0.283	↑

Gene	Gene Oncology Category Group	Gene Full name	p	FDR	AD
STX7	SYN	syntaxin 7	0.02[t]	0.181	↓
ERCC1	TF	excision repair cross-complementing rodent repair deficiency, complementation group 1	0.0003	0.052	↑
NGFB	NT	nerve growth factor β	0.03[t]	0.233	↑
NRP1	NT	neuropilin 1	0.03[t]	0.233	↑
IGF2R	NT	insulin-like growth factor 2 receptor	0.003	0.122	↑

[t]: trend level change.

Table 6.

Quantitative PCR validation of select mRNA expression of PreC transcripts

Gene	NCI (Mean±SD) (N=9)	MCI (Mean±SD) (N=9)	AD (Mean±SD) (N=8)	p	Multiple comparison
GALR1	0.26±0.137	0.40±0.334	0.22±0.065	0.644	unchanged
BAP1	0.636±0.101	0.823±0.334	0.709±0.192	0.427	unchanged
RBM3	0.207±0.154	0.169±0.155	0.324±0.233	0.202	unchanged
RAB11A	0.308±0.103	0.380±0.046	0.423±0.047	0.016	AD>NCI
HOMER1	0.092±0.060	0.138±0.060	0.181±0.085	0.045	AD>NCI
GNG2	0.247±0.208	0.196±0.0.178	0.242±0.069	0.623	unchanged
GRM1	0.249±0.226	0.212±0.158	0.314±0.141	0.514	unchanged
SLC2A5	0.996±1.237	0.813±0.440	1.240±1.537	0.572	unchanged
TIMP1	1.823±1.874	2.531±2.125	1.586±1.358	0.451	unchanged
RPS6KB1	0.168±0.066	0.240±0.098	0.215±0.062	0.159	unchanged
CHAT	0	0	0		